Pan-active imidazolopiperazine antimalarials target the *Plasmodium falciparum* intracellular secretory pathway

Gregory M. LaMonte[1], Danushka S. Marapana[2], Nina Gnadig[3], Sabine Ottilie[1], Madeline R. Luth[1], Tilla S. Worgall[4], Frances Rocamora[1], Gregory M. Goldgof[1,5] Roxanne Mohunlal[3,6], T.R Santha Kumar[3], Jenny K. Thompson[2], Edgar Vigil[1], Jennifer Yang[1], Dylan Hutson[1], Trevor Johnson[7], Jianbo Huang[7], Roy M. Williams[1], Bing Yu Zou[1], Andrea L. Cheung[1], Prianka Kumar[1], Timothy J. Egan[6], Marcus C.S. Lee[8], Dionicio Siegel[7], Alan F. Cowman,[2] David A. Fidock[3,9] and Elizabeth A. Winzeler [1]

[1] Department of Pediatrics, University of California, San Diego, School of Medicine, La Jolla, CA 92093, United States

[2] Division of Infection and Immunity, Walter and Eliza Hall Institute for Medical Research

[3] Department of Microbiology & Immunology, Columbia University Irving Medical Center, New York, New York 10032, USA

[4] Department of Pathology and Cell Biology, Columbia University Irving Medical Center, New York, New York 10032, USA

[5] Department of Laboratory Medicine, University of California, San Francisco

[6] Department of Chemistry, University of Cape Town, Rondebosch, South Africa

[7] Skaggs School of Pharmacy and Pharmaceutical Sciences, University of California, San Diego, School of Medicine, La Jolla, CA 92093, USA

[8] Parasites and Microbes Programme, Wellcome Sanger Institute, Hinxton. CB10, 1SA, UK

[9] Division of Infectious Diseases, Department of Medicine, Columbia University Irving Medical Center, New York, New York 10032, USA

Correspondence: EAW: ewinzeler@ucsd.edu

ABSTRACT

One of the most promising new compound classes in clinical development for the treatment of malaria is the imidazolopiperazines (IZPs) class. Human trials have demonstrated that members of the IZP series, which includes KAF156 (Ganaplacide) and GNF179, are potent and effective against *Plasmodium* symptomatic asexual blood-stage infections. Unlike other commonly used antimalarials, they also prevent transmission and block future infection in animal models. Despite the identification of several *Plasmodium falciparum* resistance mechanisms including mutations in ER-localized PfCARL (PfEMP65), Acetyl-coA transporter, and PfUGT transporter, IZP's mechanism of action remains unknown.

To investigate, we combined *in vitro* evolution and whole-genome analysis in the model organism *Saccharomyces cerevisiae* with molecular, metabolomic, and chemogenomic methods, in *P. falciparum*. *S. cerevisiae* clones that resist IZP activity carry multiple mutations in genes that encode endoplasmic reticulum(ER)-based lipid homeostasis and autophagy including *elo2*, *elo3*, *sur2*, *atg15* and *lcb4*, as well as ER-based *sec66.* In *Plasmodium*, IZPs cause inhibition of protein trafficking, block the establishment of new permeation pathways and result in ER expansion. We also observe sensitization with other secretion inhibitors such as brefeldin A and golgicidin as well as synthetic lethality with PfSEC62. Our data show that IZPs target the secretory pathway and highlight a novel mechanism for blocking parasite growth and development that is distinct from those of standard compounds used to treat malaria. In addition, we provide physiological signatures and hallmarks for inhibitors that work through this mechanism of action and show that IZPs are tool compounds for studying ER-dependent protein processing in different species.

INTRODUCTION

Malaria remains the most common human parasitic disease, sickening an estimated 219 million people annually and causing an estimated 435,000 deaths worldwide[1]. Although a reduction in the malaria burden has been achieved through the combined use of public health infrastructure, vector control and increased access to medical treatment[2,3], these efforts are hindered by a variety of factors, such as the lack of an effective vaccine, increased mosquito resistance to pesticides, and the continuing emergence of drug-resistant parasite strains [4-6]. There are also now reports of resistance to nearly all current classes of antimalarials[7]. Given that an estimated 3.2 billion people live in endemic regions and are at risk for malaria,[3] new classes of antimalarial compounds will be required to combat, and ultimately eradicate this disease.

One of the most promising classes of compounds are the imidazolopiperazines (IZPs), such as KAF156[8] and its closely related analog GNF179[9], which differs from KAF156 by a single halogen substitution (F to Cl). The chemotype that led to KAF156 was first identified in a phenotypic screen designed to discover compounds with activity against parasite asexual blood stages[10]. The compound series attracted more attention when it was noted that multiple analogs were present in the library, which all showed activity in a liver stage model that predicts causal antimalarial prophylaxis[9]. Subsequent rounds of medical chemistry[11,12] led to the development of KAF156, an orally available, simple-to-synthesize compound suitable for testing in humans[8].

KAF156 shows potent activity against asexual blood (IC_{50} ~ 6 nM), hepatic (IC_{50} = 4.5 nM) and sexual stages (IC_{50} = 5 nM)[8], and is considered safe with good pharmacokinetic properties in healthy human volunteers[13]. Because the compound was able to dramatically reduce parasite numbers in patients with *P. vivax* and *P. falciparum* patients in a single agent trial[14] it has now progressed to phase IIb clinical trials (NCT03167242) where it is being tested in combination with lumefantrine. It also has impressive prophylactic activity: treating mice with a single 10 mg/kg oral dose fully protects them from mosquito-borne malaria infection. Furthermore, IZPs have gametocytocidal activity and including them in a blood meal or pretreating with IZPS prevents parasites from being transmissible to mosquitoes[8], both *in vitro* and *in vivo*. If licensed, IZPs could be clinically superior to current gold standard treatments, such as artemisinin-based combination therapies, which often just provide symptomatic relief

and neither prevent malaria from developing nor prevent its transmission. KAF156 could serve as a potent tool in the mission to eliminate this disease.

Previous studies using *in vitro* evolution and whole-genome analysis in *P. falciparum* parasites showed that resistance to IZPs is mediated by mutations in three different genes, *pfcarl*, the cyclic amine resistance transporter (PF3D7_0321900)[8,9]; *pfact*, the Acetyl-CoA transporter (PF3D7_1036800); and *pfugt*, the UDP-galactose transporter (PF3D7_1113300)[15]. GFP-tagging and localization experiments have shown that these three transmembrane transporters are all localized to the endoplasmic reticulum (ER)/Golgi apparatus in *Plasmodium*. Multiple resistance-conferring alleles have been recovered independently in *pfact* and *pfcarl*.

It is unlikely that the nonessential *pfact* encodes the target, although in human cells the *pfact* ortholog, AT-1, appears essential[15]: Parasite mutants with stop codons as well as frameshifts are readily recovered after KAF156 treatment, although these may render the parasites less fit. Like the parasite protein, the human protein is also localized to the ER where it serves to import Acetyl-CoA for use in lysine acetylation of some newly synthesized protein. Its disruption in human cells results in a proteasome-independent ERAD(II) mechanism involving the unfolded protein response and autophagy of the ER[15]. In humans, mutating lysines for some proteins such as BACE results in proteins that are retained in aggregates in the ER. Many *Plasmodium* proteins are often acetylated[16], often at conserved residues, although it is not clear that this happens in the ER and which acetyl transferases are responsible for this.

Pfugt encodes a member of the Solute Carrier 35 Family. Members of this family play a role in import of sugars to the ER/Golgi where most glycoconjugate synthesis occurs[17]. Disruption of some orthologs in worms and plants also lead to ER stress[18,19]. Although disruption mutants in *pfugt* have not been obtained in high-throughput approaches in *P. falciparum*, *pfugt* is a small gene and could have been missed for random reasons[20]. Although PfCARL appears essential[20], mutations in *pfcarl* confer resistance to unrelated compounds[21,22] and resistance-conferring mutations in *pfcarl* are located in transmembrane regions and not in an obvious catalytic site. PfCARL, although conserved in evolution, remains understudied, but its yeast ortholog, Emp65 (Endoplasmic Reticulum Membrane Protein 65) protects folding polypeptides from promiscuous degradation[23]. Mutations in all three parasite proteins may lead to slower rates of protein folding, processing and sorting.

Parasites treated with IZPs have also been subjected to metabolic profiling along with other clinical compounds with known modes of action. Allman *et al.*[24] measured changes in 113 metabolites after treatment with KAF156. These data did not show a clear metabolic perturbation, in contrast to inhibitors of cytochrome bc1, dihydroorotate dehydrogenase, PfATP4, or dihydrofolate reductase, many of which are also active in both blood and hepatic stages.

Given the clinical potential of GNF179, determining its mechanism of action could reveal important new druggable pathways, suggest synergistic drugs that could be used in combination therapies, and provide clues on possible toxicity. Here we report on a series of experiments in *P. falciparum* and *S. cerevisiae* to discern the mode of action of this important antimalarial compound series.

RESULTS

Identifying potential targets of GNF179 using *S. cerevisiae* model system genetics. For target identification, we first used *in vitro* evolution studies in the model system *Saccharomyces cerevisiae*, a strategy that has been used to discover the target of cladosporin, a tRNA synthetase inhibitor that acts against both *P. falciparum* and *S. cerevisiae*. IZPs are moderately active against an attenuated strain of *Saccharomyces* that had been genetically modified by replacing 16 ABC multi-drug transporter genes with modified *Aequorea victoria* GFP (eGFP) and that has been dubbed the "Green Monster" [25]. Altogether 13 different, independent IZP-resistant yeast lines were created by growing the cells for a minimum of 20 generations in the presence of increasing GNF179 concentrations until resistance was observed (with a minimum 1.5x IC_{50} increase for GNF179). Clonal lines were isolated from each resistant culture and retested for sensitivity. The observed resistant strains exhibited 1.5 – 3.1-fold resistance relative to the drug-naïve Green Monster strain.

We sequenced drug-resistant genomes to an average 47.3x coverage and compared these to the drug-sensitive parent (Table S1). Excluding mutations in repetitive elements, we detected 67 total variants including 49 missense, frameshift or nonsense variants, 2 synonymous variants, 2 inframe deletions and 14 intergenics (Table S2). The high proportion of coding to silent mutations suggests that most changes have a beneficial effect. Multiple independent alleles were found in six different genes arising in independent selections (*sec66*(2 variants), *elo2*(5), *lcb4*(3),

YMR102C(4), *atg15*(4) and *sur2*(3)), with the most resistant lines harboring multiple mutations (e.g. GNF179-R19g2 with YMR102C, *atg15* and *sur2*) although not generally in catalytic domains (Figure 1a). With ~5800 genes in the genome, the probability of finding more than one allele by chance in the same gene after *in vitro* evolution is very low (p = 4.4 e -7) and highlights the reproducibility of the selections. In addition, the set of 38 variants included singletons in the closely related genes *sur1*, *elo3*, and *atg22*. This mutational pattern is specific to IZPs and has not been observed for *in vitro* evolution with other antimalarial compounds whose targets have been identified using the Green Monster system[26,27].

With the exception of YMR102C, whose function is not known, these genes are all directly or indirectly associated with trafficking and processes in the ER (Figure 1b). *SEC66* encodes a non-essential subunit of the SEC63 complex that forms a channel competent for SRP-dependent and post-translational SRP-independent protein targeting and import into the ER. *SEC66* disruption is well known to slow the process of protein trafficking, such that trafficking intermediates become evident by gel electrophoresis[28]. Similarly, *ELO2 and ELO3*, which encode fatty acid elongases that contribute to sphingolipid biosynthesis in the ER, were identified in a protein trafficking screen: Alleles in both *ELO2* and *ELO3*, named *VBM1* and *VBM2,*[29] were identified as suppressors of a v-SNARE mutant in which yeast cells accumulate post-Golgi secretory vesicles, and are defective in invertase secretion.[30] *ATG15* and *ATG22* play a role in autophagy, which is induced in proteasome-independent ER expansion that results from aggregates of misfolded proteins. *SUR1* (the catalytic subunit of mannosylinositol phosphorylceramide (MIPC) synthase that is required for biosynthesis of mature sphingolipids), *SUR2* (sphingosine hydroxylase involved in sphingolipid metabolism), and *LCB4* (sphingoid long-chain base kinase) are all part of the sphingolipid metabolism pathway, which is carried out in the ER. Sphingolipids and long chain fatty acids play a role in regulating autophagy. The identification of resistance-conferring genes whose products are localized to the ER or Golgi is similar to observations in *P. falciparum*.

As these resistant strains often harbored multiple mutations, we used CRISPR-*Cas9* based genome editing to introduce these mutations in a drug-naïve Green Monster genetic background. For *sec66* (M1I, IC_{50} = 70.1 µM, S107*, IC_{50} = 74.82 µM), *elo2* (G183C IC_{50} = 88.15 µM) and *elo3* (Y307*, IC_{50} = 76.56 µM) vs wild-type (WT) Green Monster IC_{50} = 47.3 µM (Table 2), the CRISPR-edited lines exhibited similar, 1.5 to 1.9-fold levels of resistance to

the drug-pressure derived lines, indicating that these three genes were responsible for the resistance observed in those yeast strains.

Some of the mutations (e.g. *elo2*, *sur2*, *atg15* and *sec66*) were early stop codons and therefore resulted in truncated proteins. To provide a further layer of confirmation for the *in vitro* resistance experiments, the homozygous deletion strains (which are not attenuated like the Green Monster strain) [31,32] for *sec66, sur2, atg15* and *elo2* were tested against GNF179, revealing each to be 1.3-2.1-fold more resistant to IZPs (IC_{50} = 121 µM (WT) vs 188 µM (*sec66*Δ), 255 µM (*elo2Δ*) and 217 µM (*sur2Δ*) respectively). We found that the homozygous deletion strain for *yer140w* (which encodes the PfCARL homolog EMP65[33]) showed low-level resistance to IZPs (152 µM), and a homozygous deletion of *sec72*, another nonessential subunit of the complex for importing proteins into the ER, also conveyed a similar level of resistance (177 µM) (Table 3). These data suggest that modifications to either the protein export complex or lipid synthesis pathways or both can result in IZP resistance in yeast. Although the observed mutations may help overcome GNF179 treatment, it seems unlikely that these genes encode targets. Many genes are not essential and we observe stop codons. In addition, levels of resistance for isolated alleles are mild.

***pfcarl* mutant lines show altered sphingolipid profiles.** To explore sphingolipid synthesis as a direct mechanism of action, we used a HPLC (high pressure liquid chromatography) linked to triple quadrupole mass spectrometry (LC-MS/MS) to measure 19 classes of sphingolipids in *P. falciparum* Dd2 parasites exposed to 5x IC_{50} (30 nM) GNF179 for 4 hours. Of note, prior work has demonstrated mammalian-like sphingolipid biosynthetic activities in *Plasmodium* parasites[34]. Results with Dd2 WT parasites were compared to the *pfcarl* triple mutant (KAD452-R3; M81I, L830V and S1076I). LC-MS/MS analysis of saponin-lysed parasite extracts identified dihydroceramides (DH), ceramides (C), sphingosines (So), sphinganines (Sa) and sphingomyelins (SM), with varying fatty acid chains and degree of saturation (Figure 2).

Normalized lipidomic comparison of untreated wild-type and mutant parasites indicated that the baseline sphingolipid concentration was notably lower in the *pfcarl* mutant. As an example, C18:1 dihydroceramide was undetectable in mutant parasites. Likewise, ceramide levels (**Figure 2b**) in untreated wild-type parasites were found to be consistently higher than in the mutant, with statistical significance being observed in 3 out of the 6 identified species (C16,

206 C20, C24). Notably, sphingomyelins (SM C18, SM C18:1) were significantly lower compared to
207 Dd2. These consistent differences observed in the *pfcarl* mutant line are supportive of shared
208 mechanisms of resistance to GNF179 between *Plasmodium* and yeast.

209 Dihydroceramides (Figure 2a) in drug-treated WT and *pfcarl* mutant parasites tended to
210 decrease and increase in concentration, respectively, compared to the untreated parasites. The
211 increase in *pfcarl* mutants upon GNF179 treatment was significant for the species C24 and
212 C24:1. Sphingosines and sphinganines (Figure 2c) demonstrated consistent trends in the
213 sphingolipid profile in that a slight decrease was observed when wild-type parasites were treated
214 with drug. The mutant exhibited a slightly different profile in that when treated, the sphingolipids
215 So and Sa increased but So-1-P and Sa-1-P either remained the same or decreased slightly in
216 concentration. None of the trends observed, however, attained statistical significance.
217 Sphingomyelins (Figure 2d) showed no significant changes upon treatment of either WT or
218 mutant parasites.

219 **Localization of GNF179 within the parasite.** To gain further insight into the
220 compound's function we next examined subcellular localization using a fluorescently-conjugated
221 form of GNF179 in *P. falciparum*, as recently performed for primaquine[35]. We first generated
222 both NBD- or Coumarin-1-conjugated forms of GNF179 (Figure 3a), leveraging an existing
223 reaction series[36]. These modified compounds retained activity against *P. falciparum* blood
224 stages, though the potency was noticeably reduced for the Coumarin-1 conjugated form of
225 GNF179 (19 nM for NBD and 1.2 μM Coumarin-1 vs 5 nM for non-modified GNF179).
226 However, the GNF179-resistant strain (KAD452-R3) was also resistant to the modified forms of
227 GNF179 (Figure 3b), indicating a similar mechanism of action for the labeled and unlabeled
228 compounds. We first examined the localization of GNF179 in ring-stage parasites, as previous
229 reports indicated that GNF179 is most active against early blood stages[22]. GNF179 colocalized
230 with ER tracker Red, a live-cell dye that recognizes the ER[37] (Figure 3c). This, combined with
231 the *S. cerevisiae* data and the localization of the three previously identified resistance genes
232 (*pfact*, *pfugt* and *pfcarl*) to the ER/Golgi, suggest that IZPs affect a process within this
233 compartment.

234 **GNF179 inhibits protein export in *P. falciparum***. To further explore the hypothesis
235 that GNF179 blocks the production or sorting of mature proteins, we next tested for synergy with

known protein-export inhibitors. Brefeldin A inhibits Sec7-type GTP-exchange factors (GEFs) that catalyze the activation of a small GTPase called Arf1, responsible for ER to Golgi transport, as well as Golgi to ER retrograde transport, through the inhibition of COPI coating of secretory vesicles[38], and is commonly used to inhibit protein secretion. We observed that treating parasites with sublethal concentrations of brefeldin A (1μM) rendered parasites 5-fold more sensitive to GNF179 (IC_{50} of 0.6 nM, vs 3 nM without brefeldin A co-treatment) (Table 4), while sensitivity to the control drug artemisinin was unchanged. This suggests that parasites exposed to GNF179 are highly sensitive to alterations in protein export.

A similar effect was observed for golgicidin, another inhibitor of protein export that works through inhibition of Golgi function[39]. Simultaneous treatment with 5 μM golgicidin (IC_{50} 11μM) also rendered parasites 2-3-fold more sensitive to GNF179 (Table 4). Importantly, this effect was specific to GNF179, rather than merely a sign of generalized parasite growth impairment, as artemisinin, atovaquone and chloroquine all showed no synergy with any of these three compounds. This synergistic effect was exclusive to inhibitors of protein secretion from the ER and Golgi, as simultaneous treatment with thapsigargin, which inhibits PfATP6 and causes depletion of ER calcium levels leading to downstream inhibition of ER chaperones[40], caused no change in GNF179 potency. In addition, we tested for synergy between GNF179 and inhibitors of the *P. falciparum* proteasome (Table 4), to determine whether the identified increase in ubiquitinated proteins was directly involved with the efficacy of GNF179 or rather was a downstream consequence. We did not observe any synergy between GNF179 and carmaphycin B, a natural product-derived proteasome inhibitor[27]. This is in contrast to artemisinin, which increases the potency of carmaphycin B. This indicated to us that the increase in protein ubiquitination was a secondary effect of GNF179 inhibiting protein trafficking, rather than a direct cause.

To examine whether protein secretion was being blocked, we sequentially looked at protein processing in *P. falciparum*. In free-living organisms, proteins are trafficked to membranes or to the extracellular environment. In intracellular malaria parasites, however, proteins can be further exported into the infected red blood cell (RBC) or hepatocyte via the PTEX complex, a parasite-specific secretory complex located in the parasitophorous vacuole membrane[41]. To examine these two processes, we used two different transiently-expressed reporters. The first reporter (Figure 4a) is based on a PfEMP3-GFP fusion protein and includes

the first 82 amino acids of PfEMP3 (PF3D7_0201900) fused to GFP. *pfemp3* encodes *P. falciparum* Erythrocyte Membrane 3, a protein that is exported to the surface of the infected RBC and that is needed to form knobs that permit cellular adhesion to vascular endothelial cell surface receptors. These 82 amino acids of PfEMP3 include both the signal peptide and PEXEL motif, a 5 amino acid sequence (RxLxE/Q/D) present in most *Plasmodium* proteins exported to the RBC cytosol. This sequence is cleaved by Plasmepsin V, a type I integral membrane-bound protease with the active domain located on the luminal side of the endoplasmic reticulum (ER).[42] Based on where the export pathway is blocked three different potential protein products may be observed, the full length fusion protein, the PEXEL-domain cleaved protein, and mature GFP. As a control, we used WEHI-842, a peptide mimetic Plasmepsin V inhibitor (EC_{50} = 400 nM)[42]. Treatment with WEHI-842 showed a marked accumulation of the full-length, unprocessed protein relative to the untreated control, as expected, given the role of Plasmepsin V in cleavage of PEXEL signal sequences. Parasites treated with high doses of GNF179, on the other hand, showed a marked decrease in levels of all forms of the secreted reporter construct, with little evidence of cleavage (Figure 4a). In contrast, levels of HSP70 protein, which does not have a signal sequence, were unchanged after treatment with GNF179 or WEHI-842. This finding suggests that proteins trafficked through the ER, but not cytoplasmic proteins, are being degraded or potentially not being synthesized due to exposure to GNF179.

The second reporter construct was a SERA5ss-GFP fusion, containing the signal peptide of SERA5 (PF3D7_0207600) fused to GFP (Figure 4b). SERA5 is an exported serine protease that plays a role in parasite egress from the infected RBC[43]. This fusion protein is co-translationally inserted to the ER and the signal peptide is removed by a signal peptidase, leading to trafficking of the mature protein to the parasitophorous vacuole (PV)[43]. SERA5ss-GFP is therefore used as a marker of protein secretion to the PV, versus the infected RBC. Without treatment, we observed two protein products for this chimera using GFP antibodies. After exposure to GNF179, the reporter showed a marked decrease in overall abundance relative to the HSP70 control, as observed for PfEMP3 reporter above (Figure 4b). In addition to marked overall reduced expression, we also observed an accumulation of the unprocessed reporter protein, based on the overall ratio of the two products. Based on results with these two reporter systems, we speculated that there was an impairment of protein secretion that occurs before signal peptide cleavage, leading to degradation of the uncleaved products or potentially a block

in synthesis. Although this could be a result of reduced total protein synthesis, we observed continued incorporation of ^{35}S methionine after treatment with GNF179, in contrast with cycloheximide. Thus, if protein synthesis was inhibited, it was likely to only be for a subset of proteins. To test whether the loss of reporter signal via western blot could be due enhanced proteolysis through the ubiquitin system we compared the effects of MG132, a proteasome inhibitor, on cleaved and uncleaved reporter levels both in the presence and absence of GNF179. These data showed that proteasome inhibition, in contrast to GNF179 inhibition, did not affect the levels or processing of either the PfEMP3 or the SERA5 reporter and that there was no observed synergy with GNF179 (Figure S1). Interestingly, increases in total ubiquitinated proteins were observed after both MG132 and GNF179 treatment, although banding patterns were somewhat different suggesting that different classes of proteins could be ubiquitinated after treatment with the two compounds.

We also tested whether native parasite proteins that are normally exported to the surrounding infected RBC would be retained within the parasite after exposure to GNF179. We therefore examined the intracellular levels of three PEXEL-containing proteins: PTP2 (PF3D7_0731100), PIESP2 (PF3D7_0501200) and SERA5 (PF3D7_0207600). In all three cases, after a short, 3-hour exposure with 10μM GNF179 (same conditions as above for the reporters for both GNF179 and WEHI-842) (Figure S2), we observed a modest accumulation of all three proteins suggesting impairment of protein export from the parasite (Figure S2). A conditional knockdown of PfSEC62 using the glmS ribozyme system[44,45] showed that parasites were 3-fold more sensitive to GNF179 (0.66 nM for 3D7 wildtype vs 0.24 nM for PfSEC62 kd) (Figure S3).

Finally, we validated the effect of GNF179 on parasite protein export in live parasites through two parallel strategies, using brefeldin A (BFA) as a positive control: visualization of export of fluorescent reporter proteins, and examination of functional phenotypes that would result from inhibition of protein secretion. To begin, we constructed a parasite strain that bears a fusion between the Knob-Associated Histidine Rich Protein and GFP[44] (Figure 5a). The chimeric gene, which bears the first 69 amino acids of KAHRP containing the signal peptide (SP) and PEXEL motif (Px), was expressed from a *pfcrt* promoter and was integrated into the *cg6* locus in Dd2-attB parasites using the attP × attB integrase system[45]. In the absence of GNF179 the GFP

reporter was trafficked to the parasitophorous vacuole (PV) as well as to the RBC cytosol, as shown by the GFP staining in the PV surrounding the parasite (Figure 5b). In contrast, treatment with brefeldin A resulted in accumulation of the GFP reporter in the parasite ER as evidenced when co-staining with an anti-PDI antibody (cyan) or by using ER tracker red (Figure 5b and Figure S4). The white dotted outlines indicate overlap of green and cyan labels. To better understand in which subcellular compartment the export block occurred we co-stained with antibodies to both the cis-Golgi resident protein, ERD2,[46] and to the ER (PDI)). In contrast to BFA - treated parasites, images of parasites treated with 5x IC_{50} GNF179 (25 nM) for 16 hours showed colocalization of the GFP signal at times with both organelles (Figure 5c), although we found more colocalization with the ER than with the Golgi (area circles with white dotted lines). Interestingly, staining of parasites with ER-tracker after GNF179 treatment showed an expansion of ER tracker positive space relative to nuclear staining (Figure S4 a-c). 3D volume quantification of the ratio between DAPI-positive staining to ER-staining in live, GNF179-treated parasites showed a statistically-significant expansion of the ER (Figure S4d).

To functionally confirm a secretion defect, we next determined whether parasites treated with GNF179 would be less sensitive to sorbitol treatment, which kills mature parasites and is used to synchronize cultures as only ring-stage parasites survive. For sorbitol to kill later stage parasites, the new permeability pathways (NPPs) must first be established in the RBC, which requires the export of a network of transport proteins [49] (Figure 5e). Here, we observed that 4 hours of pretreatment with 25 nM GNF179 led to a loss of sensitivity to sorbitol, as seen via the presence of a nearly asynchronous culture 24 hours post synchronization (Figure 5f). This was in contrast to parasites that were GNF179 resistant, resulting from mutations in either *pfcarl* (KAD452-R3, Figure 5f) or, to a lesser degree, *pfact* (Dd2-ACTStop, Figure 5f). Those resistant parasites showed less protection and more sorbitol lysis. As controls we observed a similar phenotype with brefeldin A but not with chloroquine. The lack of sorbitol sensitivity in the presence of GNF179 further highlights the impairment of ER-mediated protein trafficking due to GNF179 exposure.

DISCUSSION

Once the parasite has successfully invaded the host cell, the parasite undergoes a rapid induction of protein synthesis[50]. This includes the folding and sorting of hundreds of membrane proteins and the secretion of hundreds of proteins into the host cell via the parasite ER and the PTEX complex in the PVM, leading to a dramatic rearrangement of host cell processes, all essential for parasite survival. Proteins needed for these essential processes may make effective drug targets, as shown by the development of WEHI-842, an inhibitor of Plasmepsin V[51]. In addition, KDU691 targets PI4K[52], a protein involved in a variety of processes including vesicular trafficking from the Golgi apparatus. While the trafficking of proteins into the infected RBC may only occur during the asexual blood stage, general trafficking and protein modification is a process that occurs, at least to some degree, at all stages of parasite development. Therefore, proteins that play a role in protein processing or sorting pathways would be logical targets for the type of multistage (hepatic, asexual blood and gametocyte stages) activity possessed by KAF156.

The ER serves as the initial entry into the protein trafficking and secretion pathways, as a site for protein folding, and as the location of a significant portion of the post-translation modification of parasite proteins. All of our available data suggest that KAF156 exerts its effect in this organelle, including the localization of gene products that give resistance (in both *S. cerevisiae* and *P. falciparum*) to KAF156/GNF179 as well as the localization of NBD and Coumarin-labeled compounds. The ER is responsible for many functions, including lysine acetylation, protein folding, glycosylation and sphingolipid biosynthesis (Figure S5). After proteins have been modified and folded, they are sorted to other compartments. While KAF156 may block the sorting of proteins to other compartment, our data seem more compatible with this agent working at an earlier stage, protein-production stage, possibly during protein folding: Western blot analysis shows a substantial reduction in the total amounts of secreted reporter proteins relative to cytoplasmic proteins after GNF179 treatment, suggesting that the synthesis of both membrane and PTEX-trafficked proteins may be disrupted. The reduction in protein levels is in contrast to using the WEHI-842 inhibitor of the ER-based Plasmepsin V export protease, where a shift from the processed to the unprocessed form of the protein is observed yet protein reporter levels stay high. Levels of proteins that are not exported to the RBC but have a simple signal sequence are also reduced (Figure 4).

While a block in the synthesis of membrane proteins might be expected to result in an unfolded protein response, and synergy with proteasome inhibitors such as carmaphycin B, there

388 are different degradation pathways for cytoplasmic proteins versus proteins that are destined to
389 be secreted. Recent data reveal the existence of two pathways for dealing with protein aggregates
390 in the ER: ERAD(I) and ERAD(II)[53]. The second pathway depends on autophagy and lysosomal
391 trafficking for the disposal of large protein aggregates, and is observed in human cells when
392 Acetyl-CoA Transporter is disrupted[54]. It is likely that ERAD(II) is used when secreted reporters
393 (e.g. KAHRP69-GFP) are overexpressed, as we observed no great increase in ubiquitinated
394 proteins after GNF179 treatment except when a proteasome inhibitor (MG132) was used in
395 combination with GNF179 (Figure S1). An expansion of the ER, similar to that observed after
396 GNF179 treatment in malaria parasites (Figure S4), is observed when yeast cells are treated with
397 agents that induce the unfolded protein response. ER expansion induces autophagy as a
398 mechanism to deal with ER-stress and eliminate the blockage[55].

399 Although GNF179 appears to work in the ER, the exact target of GNF179 is not known.
400 On the other hand, the cancer and antinfectives drug discovery communities have explored this
401 organelle and its processes for targets (reviewed in [56]). The ER protein-folding factory examined
402 here also holds targets for antivirals as viruses need to be packaged within the ER[56]. In addition,
403 it has been established that the *P. falciparum* Signal Peptide Peptidase PfSPP1 is a drug-able
404 target and its inhibition results in parasite death across the lifecycle[57]. Conservation of critical
405 targets across species seems to be more the rule than the exception although selectivity of
406 inhibitors may be very different.

407 Although it is difficult to predict a target based on chemical structure, KAF156 has
408 structural features that suggest it may inhibit a kinase or other ATP or GTP binding proteins.
409 Many potential essential targets with ATP or GTP binding pockets are present ER-dependent
410 protein packaging pathway. Members of the Sec62 translocon complex could be possible targets.
411 However, Sec62 does not have an obvious catalytic site, a feature that is associated with many
412 targets, although it is possible that IZPs are allosteric inhibitors. Signal recognition particle
413 (SRP) is a protein complex critical for the translocation of proteins into the ER [58]. Within this
414 complex, both SRP54 and SRPα harbor GTPase domains, both of which would represent a prime
415 drug-able target. However, these data would not explain the increased ER volume that is
416 observed with GNF179-exposed parasites. Other candidates may include heatshock proteins
417 such as the GRP94-like protein endoplasmin (PF3D7_1222300). This essential protein has an
418 ATP-binding domain and selective targeting with small molecule inhibitors is possible[59].

GRP94 homologs are not found in yeast and bacteria. However, GRP94 is somewhat homologous to HSP82. In fact, in our yeast selections we detect a Ser to Ile substitution at position 17 that lies in proximity to the ATP-binding pocket. However, the lack of a close ortholog may explain the 10,000-fold difference in potency in the yeast model. In addition, binding immunoglobulin protein (BiP), the Hsp70 homologue within the ER (PF3D7_0917900), requires ATPase activity to perform the final step of protein translocation from the SEC61 translocon into the ER[60] and could also be a plausible target. Chemical targeting of BiP is feasible.[61] The hypothesis that KAF156/GNF179 targets protein folding in the ER is supported by the role of EMP65 as a guardian factor that protects newly synthesized, unfolded polypeptides from degradation (See Figure S5 for model). If *pfcarl-emp65* is mutated, more premature degradation may occur in the presence of GNF179/KAF156, which may allow the cells to tolerate 10X more GNF179.

Another potential class of proteins are Rab GTPases. Given the synergy we observed between GNF179 and brefeldin A, GNF179 could inhibit COPI-mediated transport from the ER to the Golgi, similar to the mechanism of action of brefeldin A[62]. Sar1, an essential gene involved in the Sec23 complex, for example, is a small GTPase that functions as a target in a yeast brefeldin suppressor screen[62]. The lysine transferase that adds acetyl groups to nascent peptides, helping them fold and which relies on PfACT activity could be a target.

Protein glycosylation in the ER may could also be inhibited and may lead to unfolded aggregates within the ER. Tunicamycin, a nucleoside analog, inhibits protein N-linked glycosylation by preventing core oligosaccharide addition to nascent polypeptides by binding to UDP-N-acetylglucosamine--dolichyl-phosphate N-acetylglucosamine phosphotransferase (Alg7). Tunicamycin thereby also blocks protein folding and transit through the ER. The *P. falciparum* version of Alg7, PF3D7_0321200, could theoretically be a target, although the structure of KAF156 is not similar to tunicamycin.

It is although worthwhile noting that several additional compounds may work via similar or related mechanisms. For example, mutations in *pfcarl* are acquired when parasites are treated with sublethal concentrations of MMV007564[63]. In particular, if there is a *pfcarl* or *pfact* resistance mechanism, it seems likely that protein folding or trafficking in the ER is targeted. More work will be needed to determine whether MMV007564 has the same target as KAF156 or

449 if they are only in the same pathway. By comparison, there are a variety of different chemotypes
450 that inhibit mitochondrial function[64], as well as different chemotypes that interact with the same
451 active site, however there still seem to be a limited number of high-value inhibitor binding sites
452 in this pathway, and they appear repeatedly.

453 An additional mechanism of action for IZPs could be inhibiting the process of ER
454 autophagy. The mammalian orthologue of Sec62, potentially a target of GNF179, is required for
455 the degradation of excess ER components in a process termed ER autophagy[65]. *In vitro* directed
456 evolution of *S. cerevisiae* using GNF179 identified mutations in the *atg15* and *atg22*, genes that
457 play a role in ER-autophagy. In addition, GNF179 induced an expansion in ER size upon
458 treatment of *P. falciparum*. Collectively, these results suggest that IZPs affect ER homeostasis
459 and function by inhibiting proteins critical for ER-phagy.

460 Strategies for finding the target of KAF156 remain limited in the absence of genetic
461 methods, and few antimalarials have been matched with their target when genetic methods fail.
462 Affinity-based methods were used to match MMV030048 to PI4K with success[66], although such
463 strategies required the use of a modified ligand. Cellular Thermal Shift Assays (CETSA)
464 methods that involve incubating total cellular extracts with an unmodified ligand and identifying
465 those proteins that resist heat denaturation in the presence of compound is a strategy that shows
466 promise[67]. Another potential option involves a genome-wide knockdown or knock-in libraries,
467 which have been used with success in trypanosomes and to find the target of cladosporin also
468 using the *S. cerevisiae* model[68]. A limitation of all of these genome-wide methods is that they
469 may produce hundreds of possible candidate molecules, and it can be challenging to sort through
470 them using the slow methods available in *Plasmodium*. While finding the exact target may
471 require some work, the studies here should allow prioritization of candidates that are identified in
472 genome-wide experiments.

473 ## MATERIALS AND METHODS

474 ### *In vitro* Resistance Evolution and Whole Genome Sequencing of GNF179-resistant *S.*
475 ### *cerevisiae*

476 Sublethal concentrations of GNF179 were added to 50ml conical tubes containing 20µl
477 of saturated *S. cerevisiae* ABC_{16}-Monster cells in 20ml of YPD media. Each selection was
478 cultured under vigorous shaking until the culture reached saturation. Saturated cultures were

diluted into fresh YPD media containing increasing GNF179 concentrations, and multiple rounds of selection were performed. Cells of cultures that were able to grow in substantially higher drug concentrations than the parental cell line, were streaked onto agar plates containing GNF179 to select for single colonies. Single colonies were isolated, and IC_{50} assays, prepared by two-fold dilution were performed to determine the degree of evolved resistance vs. that of the parental strain.

Genomic DNA (gDNA) was extracted from yeast samples using the YeaStar Genomic DNA kit (Cat. No D2002, ZYMO Research). Sequencing libraries were prepared using the Illumina Nextera XT kit (Cat. No FC-131-1024, Illumina) following the standard dual indexing protocol, and were then sequenced on the Illumina HiSeq 2500 in RapidRun mode to generate paired-end reads 100bp in length. Reads were aligned to the *S. cerevisiae* 288C reference genome (assembly R64) using BWA-mem[69] and further processed using Picard Tools (http://broadinstitute.github.io/picard/). A total of 13 clones were sequenced to an average coverage of 47.3x, with an average of 99.3% of reads mapping to the reference genome. SNVs and INDELs were called using GATK HaplotypeCaller, filtered based on GATK recommendations[70] and annotated with SnpEff[71]. Variants were further filtered by removing mutations that were present in the both drug-sensitive parent strain and resistant strains, such that mutations were only retained if they arose during the drug selection process.

CRISPR-*Cas*9 Allelic Exchange in *S. cerevisiae*

CRISPR-*Cas*9 genome engineering was performed on the *S. cerevisiae* ABC_{16}-Monster strain using vectors p414 and p426 obtained from the Church lab (Addgene) as previously described[72]. To produce gRNA plasmids specific to the desired mutation sites, oligonucleotides were synthesized (Integrated DNA Technologies) to match the target sequence and contain a 24 base-pair overlap with the p426 vector backbone. Gene-specific gRNAs were amplified by PCR, transformed into Stellar™ competent *E. coli* cells (Takara) and selected on LB-Ampicillin plates. DNA was isolated from transformed *E. coli* cells and purified using the QiaQuick Miniprep kit (Qiagen) and quantified via Qubit Fluorometric Quantitation (ThermoFisher). Cas9-expressing ABC_{16}-Monster cells were transformed with 300-500ng of gene-specific gRNA vector and 1-2 nmole of synthesized donor template (IDT) containing the desired base-pair substitution via standard lithium acetate method. Transformed cells were selected on methionine and leucine

deficient CM-glucose plates. Each mutation was confirmed with Sanger sequencing (Eton Bioscience).

P. falciparum culture

P. falciparum Dd2 strain parasites were cultured under standard conditions[73], using RPMI media (Thermo Fisher # 21870076) supplemented with 0.05 mg/ml gentamycin (Thermo Fisher # 15710072), freshly-prepared 0.014 mg/ml hypoxanthine (Sigma Aldrich #H9377), 38.4 mM HEPES (Sigma Aldrich #H3375), 0.2% Sodium Bicarbonate (Sigma Aldrich #S5761), 3.4 mM Sodium Hydroxide (Sigma Aldrich #S8045), 0.05% O+ Human Serum (Denatured at 56^0C for 40 min and obtained from Interstate Blood Bank, Memphis, TN) and 0.0025% Albumax (Thermo Fisher Scientific # 11021037). Human O+ whole blood was obtained from The Scripps Research Institute (La Jolla, CA) using the Normal Blood Program and Humann Subjects Protocol Number (IRB-12-5933). Leukocyte-free erythrocytes were stored at 50% hematocrit in RPMI-1640 screening media (as above, but without O+ human serum and with 2x albumax concentration) at 4°C for one to three weeks before experimental use. Cultures were monitored every one to two days via direct observation of parasite infection using light microscopy-based observation of Giemsa-stained thin blood smears of parasite cultures. Specific parasite cultures used are as indicated in the specific experiments.

Conjugation of Coumarin-1 and NBD with GNF179

GNF179 was conjugated with a coumarin-1 fluorophore as previously described[36]. Briefly, Meldrum's acid was acylated with methyl 5-chloro-5-oxovalerate and subsequently treated with methanol to provide coumarin β-keto ester. Next, the β-keto ester was first reacted with resorcinol under acidic conditions and then hydrolyzed with lithium hydroxide to provide 4-(7-hydroxy-2-oxo-2H-chromen-4-yl) coumarin butanoic acid 2.8 Finally, GNF179 and coumarin butanoic acid was coupled under standard EDCI/DMAP coupling conditions to yield the probe Coumarin-1-GNF179. To construct the NBD modified version, GNF179 was conjugated with a nitrobenzoxadiazole (NBD) fluorescent label by reacting GNF179, triethylamine, and commercially available NBD-Cl in dimethylformamide.

All reactions were performed in flame- or oven-dried glassware sealed with rubber septa and under nitrogen atmosphere, unless otherwise indicated. Air- and/or moisture-sensitive liquids or solutions were transferred by cannula or syringe. Organic solutions were concentrated by rotary

evaporator at 30 millibar with the water bath heated to not more than 50°C, unless specified otherwise. Thin-layer chromatography (TLC) was performed using 0.2 mm commercial silica gel plates (silica gel 60, F254, EMD Chemicals). Nuclear Magnetic Resonance (NMR) spectra were recorded on a Varian (^{1}H NMR: $CDCl_3$ (7.26) at 600 MHz; ^{13}C NMR: $CDCl_3$ (77.16) at 151 MHz). All spectra were taken in $CDCl_3$ with shifts reported in parts per million (ppm) referenced to protium or carbon of the solvent (7.26 or 77.16, respectively). Coupling constants are reported in Hertz (Hz). Data for ^{1}H-NMR are reported as follows: chemical shift (ppm, reference to protium; s = single, d = doublet, t = triplet, q = quartet, dd = doublet of doublets, m = multiplet, coupling constant (Hz), and integration). High Resolution Mass Spectra (HRMS) were acquired on an Agilent 6230 High Resolution time-of-flight mass spectrometer and reported as m/z for the molecular ion [M+H]+.

GNF179-1-Coumarin

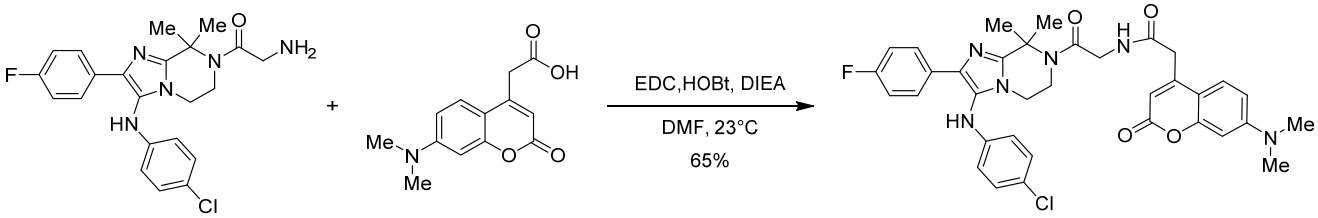

GNF179 GNF179-1-Coumarin

GNF179-1-Coumarin: A dry 5 mL round-bottom flask equipped with a stir bar, sealed with a rubber septum was charged with 7-dimethylaminocoumarin-4-acetic acid (4 mg, 0.016 mmol, 1.0 equiv.) and GNF179 (7 mg, 0.016 mmol, 1.0 equiv.) in dry DMF (0.2 mL). The solution was cooled to 5 °C and solid EDC (4 mg, 0.023 mmol, 1.42 equiv.), HOBt (3 mg, 0.019 mmol, 1.2 equiv.) and neat DIEA (3 µL, 0.019 mmol, 1.2 equiv.) were added to the mixture. The solution as stirred for 30 mins and the reaction was allowed to warm to ambient temperature and react for 18 hours. The reaction was then diluted with EtOAc (3 mL) and washed with water (1 mL). The mixture was extracted with EtOAc (2 mL). The combined organic layers were dried over sodium sulfate, filtered, and concentrated. The crude product was purified by silica column chromatography, eluting with Hexanes: EtOAc (10: 90) affording the title compound (6 mg, 9.13 mmol, 63%) as yellow color solid.

NMR results: $\mathbf{R_f}$ = 0.5 (silica gel, 100 EtOAc); **^{1}H NMR** (600 MHz, $CDCl_3$) δ 7.73 (dd, *J* = 8.5, 5.6 Hz, 2H), 7.40 (d, *J* = 9.0 Hz, 1H), 7.13 (d, *J* = 8.6 Hz, 2H), 6.95 (m, 3H), 6.56 (m, 3H), 6.35 (d, *J* = 2.1 Hz, 1H), 6.01 (s, 1H), 5.79 (s, 1H), 4.06 (d, *J* = 3.7 Hz, 2H), 3.68 – 3.64 (m, 2H), 3.63 (s, 2H), 3.47 (m, 2H), 3.00 (s, 6H), 1.88 (s, 6H). **^{13}C NMR** (151 MHz, $CDCl_3$) δ 167.98, 167.27, 162.70, 162.02, 161.07, 155.94, 153.11, 149.83, 147.44, 144.32, 133.72, 129.74, 127.64, 127.59, 125.60, 124.46, 122.96, 115.50, 115.36, 114.57, 110.15, 109.20, 108.41, 98.12, 60.34, 43.51, 41.69, 41.01, 40.17, 39.89, 26.47. **HRMS**: *m/z*: calcd for $C_{35}H_{35}ClFN_6O_4$: 657.2387; found 657.2384 $[M + H]^+$.

GNF179-NBD

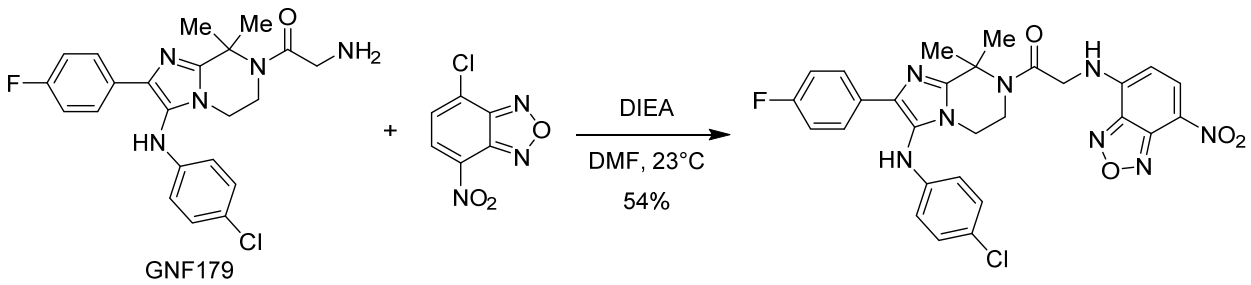

GNF179-NBD: To a stirred solution of GNF179 (6 mg, 0.014 mmol, 1.0 equiv.) and 4-chloro-7-nitrobenzofuran (3 mg, 0.014 mmol, 1.0 equiv.) in dry DMF (0.2 mL) was added neat DIEA (4 µL, 0.021 mmol, 1.5 equiv.). The solution was stirred for 16 hours at 23 °C. The reaction was then diluted with EtOAc (2.5 mL) and water (1.2 mL) and the organic layer was collected. The mixture was extracted with additional EtOAc (2 mL). The EtOAc layers were dried over sodium sulfate, filtered, and concentrated. The crude product was purified by silica column chromatography, eluting with Hexanes: EtOAc (40: 60) afforded the title compound (4 mg, 6.77 mmol, 52%) as light brown solid.

NMR results: $\mathbf{R_f}$ = 0.6 (silica gel, 30:70 Hexanes: EtOAc); **^{1}H NMR** (600 MHz, $CDCl_3$) δ 8.35 (d, *J* = 8.4 Hz, 1H), 7.72 – 7.65 (m, 2H), 7.59 (s, 1H), 7.13 (d, *J* = 8.2 Hz, 2H), 6.94 (t, *J* = 8.3 Hz, 2H), 6.57 (d, *J* = 8.2 Hz, 2H), 6.13 (s, 1H), 5.60 (s, 1H), 4.30 (s, 2H), 3.91 (m, 2H), 3.80 (m, 2H), 2.00 (s, 6H). **^{13}C NMR** (151 MHz, $CDCl_3$) δ 162.72, 161.08, 147.27, 144.22, 133.82,

129.81, 129.65, 129.64, 127.67, 127.62, 124.62, 122.93, 115.53, 115.38, 114.59, 60.93, 56.09, 41.95, 41.03, 29.80, 26.52. **HRMS**: *m/z*: calcd for $C_{28}H_{25}ClFN_8O_4$: 591.1666; found 591.1662 $[M + H]^+$.

The potency of both GNF179 fluorescent conjugate was assessed via a 72-hour SYBR Green I fluorescence IC_{50} assay.[74]

Sphingolipid Quantitation

Parasites were grown in culture media containing both human serum (5%) and albumax (0.25%) at 3% hematocrit. Asynchronous parasites (containing ~2/3rd rings) were treated with GNF179 for 4 hours at 5X wild type IC_{50} (25nM). Parasitized cells were then washed with PBS (+ drug for GNF179-treated samples). Samples were then lysed with 5 volumes of 0.15% saponin (in cold PBS) on ice for 20min, and centrifuged and washed extensively. Parasite pellets were flash frozen in liquid nitrogen and stored at -80°C until use.

Protein concentrations were measured using the Bradford Protein Assay for biological (n=3) and technical (n=2) replicates for WT and mutant parasites ± drug. Samples were solubilized using cell lysis buffer comprising 1M Tris, 20% SDS, 0.5M EDTA, β-mercaptoethanol and double distilled water then boiled at 95˚C for 5min. Bovine serum albumin (BSA) standards and parasite samples were incubated with Bradford Reagent (BioRad) at room temperature for 15-30min then absorbance read at 595nm in order to derive protein concentrations.

For lipid extraction, parasite samples and controls for lipid analysis were prepared in a 96 well plate comprising a final volume of 50µl per well. To each well, 50µl internal standards comprising ceramide (C12) and sphingomyelin (SM12) were added. Lipids were extracted from parasite and control samples using 900µl dichloromethane/methanol (1:1 v/v). The plate was vortexed overnight at room temperature then centrifuged to pellet out all insoluble material. The supernatant containing lipids was transferred into a new plate and samples subjected to mass spectrometry using a triple quadrupole LC-MS system. Briefly, 7µl of sample was injected into the HPLC running through a C18 Poroshell column into Agilent QQQ 6430 MS/MS. HPLC was optimized under the following conditions: mobile phase A (water/ methanol/ chloroform/ 0.1% formic acid) and mobile phase B (methanol/ acetonitrile/ chloroform/ 0.1% formic acid).

Analysis was done on Agilent Quantitative Analysis software and normalized to total protein in the samples.

All sample data sets were analyzed using Graph Pad Prism 4.0. Tables 2.1-2.19 below, show the output from Prism comparing sphingolipid content across all possible combinations of data in treated (+) and untreated (-) wild type (Dd2) and *pfcarl* mutant (KAD452-R3) parasites. Sphingolipids were normalized to protein and reported with respect to the mean ± SEM for n=3 independent experiments. Asterisks included in the tabulated data indicate statistical significance at the 95% confidence interval determined using a two-tailed t-test (* $p < 0.05$, ** $p < 0.01$, *** $p < 0.001$). n.d. denotes samples with insufficient data or lipid contents below the detection limit.

Immunoblotting to demonstrate Protein Trafficking Defects

P. falciparum parasites expressing PfEMP3-GFP or PfSERA5ss-GFP were generated as previously described[41], with the indicated reporters cloned into pGLUX.1 and their expression driven by the PfCRT promoter. *P. falciparum* trophozoites expressing PfEMP3-GFP or PfSERA5ss-GFP were magnetically-purified (Miltenyi Biotech), incubated with 10μM GNF179 or WEHI-842 for 3hrs at 37°C, and treated with 0.09% saponin-containing inhibitor. Washed pellets were solubilized in 2x Laemmli buffer (Bio-Rad #1610737) then boiled for 3 min. Proteins were then separated by SDS-PAGE, transferred to nitrocellulose and blocked in 1% skim milk. Membranes were probed with mouse anti-GFP (Roche, cat. no. 11814460001) (1:1,000) (primary validation is provided on the manufacturer's website) or rabbit anti-HSP70 (1:4,000), subsequently followed by probing with species-matched horseradish peroxidase–conjugated secondary antibodies (Cell Signaling Technology, cat. nos. 7074 and 7077) and visualization with enhanced chemiluminescence (Amersham).

For endogenous proteins, 3D7 wild-type *Plasmodium* parasites were treated with the indicated concentrations of GNF179 for 3hr at 37°C, and treated with 0.09% saponin-containing inhibitor. Immunoblotting was performed as described above using antibodies for PfIESP2, PfSERA5 and PfPTP2[75].

Sec62 knockdown assay

3D7 wild type and PfSec62-HA-glmS transgenic parasites[45] were synchronized using sorbitol at ring stage and incubated with 0 mM and 1 mM Glucosamine (Sigma). GNF179, chloroquine and

mefloquine were added at increasing concentrations and all cultures incubated for 48 hrs until the late ring stage of the successive cycle. Parasitaemia at each drug concentration was assessed by flow cytometry and all data tabulated using GraphPad Prism.

Measuring Parasite Translation using ^{35}S-Incorporation

The effect of drug treatment on parasite translation was evaluated by quantifying the incorporation of ^{35}S-labeled amino acids into newly synthesized protein by adapting a published protocol [76]. Briefly, synchronized, trophozoite-stage parasites (5% parasitemia, 26-30 hpi) were first washed in methionine-free media three times prior to drug treatment. Parasites were then incubated in various compound concentrations in 24-well plates for 1 hour at 37^{o}C, at a final hematocrit of 5%, and a final concentration of 125 µMci/mL of EasyTag™ EXPRESS^{35}S Protein Labeling Mix (Perkin Elmer, USA). Concentrations used for incubation correspond to 100-, 10-, 1-, 0.1- and 0.01-times the IC50 values of KAF156 (15 nM), chloroquine (85 nM) and cycloheximide (750 nM). After incubation, parasites were washed with 1x PBS and then lysed using ice-cold 0.15% saponin in 1x PBS for 20 minutes. All subsequent steps were performed on ice. The saponin pellet was washed with 1x PBS, and then resuspended in 0.02% sodium deoxycholate and supplemented with an equal volume of 16% trichloroacetic acid (TCA) to make a final concentration of 8% TCA. The suspensions were then incubated for 20 minutes on ice before vacuum filtration. To collect the radiolabeled, precipitated proteins, the samples were dispensed onto 0.7µM glass fiber filter discs (Millipore, USA) that had been presoaked in 8% TCA. The vacuum-filtered precipitates were then washed twice with 8% TCA and then, finally, with 90% acetone. The filter discs were allowed to air-dry for at least two hours, transferred into scintillation vials and resuspended in scintillation cocktail (Perkin Elmer, USA). ^{35}S counts were obtained for 1 minute using a Beckman Coulter LS 6500 Multi-purpose Scintillation Counter. Counts were normalized to data obtained from untreated parasites.

New Permeation Pathways Assessment of Sorbitol Synchronization Efficacy after GNF179 treatment

Parasites were cultured as above. Three parasite strains were used, wild-type Dd2, KAD452-R3 and Dd2 ACT S242* (Dd2 *act* - PF3D7_1036800 – with S242* SNV [21]). Each parasite clone was split into 3 sets of matched cultures. Each set of matched cultures was either treated for 4hr at 37°C with compound (50nM GNF179, 500nM Chloroquine or 5µM Brefeldin

A (Sigma Aldrich #B6542)) or an equal volume of DMSO. After drug treatment, cultures were synchronized by treatment with 5% sorbitol (Sigma Aldrich # 240850) for 10min at 37°C, washed once with media and returned to normal culture conditions. 24 hours after treatment, cultures were assessed by thin blood smear and GIEMSA staining for parasite lifecycle stage. The proportion of early ('ring') stage parasites to the total parasite proportion was recorded.

Microscopy Methods Parasite culture

P. falciparum asexual blood-stage parasites were cultured in human erythrocytes (3% hematocrit) and RPMI-1640 media supplemented with 2mM L-glutamine, 50mg/L hypoxanthine, 25mM HEPES, 0.225% $NaHCO_3$, 10mg/L gentamycin, and 0.5% (w/v) Albumax II (Invitrogen). Parasites were maintained at 37ºC in 5% O_2, 5% CO_2, and 90% N_2. Cultures were stained with Giemsa, monitored by blood smears fixed in methanol, and viewed by light microscopy.

Export block assay

The KAHRP69-GFP reporter line was generated by amplifying the first 207 bp of the KAHRP gene (PF3D7_0202000), which includes the signal peptide and PEXEL motif, followed by a glycine linker, and cloning upstream of GFP in the pDC2-crt-attP-BSD vector under the control of the *pfcrt* 5' UTR. The plasmid was integrated by attB x attP recombinase-mediated integration into the Dd2attB parasite line[77]. Dd2attB KAHRP69-GFP ring stage parasites were incubated with either 5×IC_{50} GNF179 (25nM), Brefeldin A (5µg/ml) (Sigma Aldrich) or DMSO-mock treated 16hr prior to imaging. For live-cell imaging, 5 µl of resuspended culture was added to 30 µl of RPMI-1640 media (without Albumax II) containing Hoechst 33342 (1µg/ml) (Sigma) and imaged at room temperature after 5min incubation at 37°C. For experiments with ER-Tracker™ Red (Thermo Fisher), the dye was added to a final concentration of 1µM 30min prior to imaging. Indirect Immunofluorescence assays (IFAs) were performed in suspension. Cells were fixed in 4% (v/v) formaldehyde (Thermo Fisher Scientific) for 1h at RT followed by a second fixation step supplementing the 4% formaldehyde solution with 1mM Cysteine and $CaCl_2$ and subsequent incubation over night at 4°C. The cells were permeabilized on ice using 0.05% Triton X-100 in 1×PBS for 5min and autofluorescence was quenched using 50 mM glycine for 10 min. After two washes in 1×PBS the cells were resuspended in 1% (w/v) bovine serum

albumin (BSA) in 1×PBS blocking buffer and incubated with the appropriate dilution for each primary antibody used (1/200 for anti-ERD2, 1/200 for anti-PDI (Mouse anti-PDI (1D3), Enzo Life Sciences, Cat. No. ADI-SPA-891-D), 1/500 for anti-GFP) followed by an incubation with the species-specific corresponding secondary antibody (Alexa Fluor 488-, 594- or 647-conjugated goat anti mouse or rabbit antibodies, Thermo Fisher) diluted 1:2000 in 1% BSA in 1×PBS.

Parasites were imaged using a Nikon Eclipse Ti-E wide-field microscope equipped with a sCMOS camera (Andor) and a Plan-apochromate oil immersion objective with 100× magnification (1.4 numerical aperture). A minimum of 27 Z-stacks (0.2 µm step size) were taken of each parasitized RBC. NIS-Elements imaging software (Version 5.02, Nikon) was used to control the microscope and camera as well as to deconvolve the images (using 25 iterations of the Richardson-Lucy algorithm for each image) and perform 3D reconstructions. ImageJ (Fiji) (version 2.0.0-rc-68/1.52h) was used to crop the images, adjust brightness and intensity, overlay channels and prepare montages.

Author Contributions

Parasite functional assays were conceived by G.L., D.M., D.A.F., A.C. and E.AW. Parasite functional assays, including gene knockdowns, drug synergy experiments and conditional knockdowns, were performed by G.L., D.M, J.K.T. and BY.Z.. Parasite *in vivo* transation assays were performed by F.R. *S. cerevisiae* resistance evolutions and functional assays were performed by E.V., J.Y., A.L.C., P.K. G.G. and S.O. Whole-genome sequencing was performed by the UCSD Institute for Genomic Medicine Core Facility and analyzed by M.L. Fluorescent compounds were synthesized by D.S, T.J. and J.H. E.A.W. wrote the manuscript. All authors read and approved the manuscript. The authors declare no conflicts of interest or competing financial interests.

Acknowledgements

The authors would like to thanks the members of the Winzeler lab for technical support, reagents and critical reading of the manuscript. GL is supported by an AP Giannini post-doctoral fellowship. E.A.W. is supported by grants from the NIH (5R01AI090141 and R01AI103058) and by grants from the Bill & Melinda Gates Foundation (OPP1086217, OPP1141300) as well as by

Medicines for Malaria Venture (MMV). DAF gratefully acknowledges funding from the Medicines for Malaria Venture and the Bill & Melinda Gates Foundation. M.L. was supported in part by a Ruth L. Kirschstein Institutional National Research Award from the National Institute for General Medical Sciences, T32 GM008666.

Data Availability

All genome sequences for the 13 IZP-resistant *S. cerevisiae* strains have been placed in the short-read sequence archive (http://www.ncbi.nlm.nih.gov/sra) under accession code STUDY: PRJNA381796 (SRP107357). Whole-genome sequences for KAD452-R3 can be downloaded from (located on NAS server: Victoria, collaborative sequencing projects, Lamonte_KAF156R)

References

1. WHO. *World malaria report 2018*, (World Health Organization, 2018).
2. Snow, R.W., Craig, M., Deichmann, U. & Marsh, K. Estimating mortality, morbidity and disability due to malaria among Africa's non-pregnant population. *Bulletin of the World Health Organization* **77**, 624-640 (1999).
3. Gething, P.W.*, et al.* A new world malaria map: Plasmodium falciparum endemicity in 2010. *Malaria journal* **10**, 378 (2011).
4. Sidhu, A.B.S., Verdier-Pinard, D. & Fidock, D.A. Chloroquine Resistance in Plasmodium falciparum Malaria Parasites Conferred by pfcrt Mutations. *Science* **298**, 210-213 (2002).
5. Suwanarusk, R.*, et al.* Chloroquine Resistant <italic>Plasmodium vivax</italic>: <italic>In Vitro</italic> Characterisation and Association with Molecular Polymorphisms. *PLoS ONE* **2**, e1089 (2007).
6. Mok, S.*, et al.* Artemisinin resistance in Plasmodium falciparum is associated with an altered temporal pattern of transcription. *BMC Genomics* **12**, 391 (2011).
7. Dondorp, A.M.*, et al.* Artemisinin resistance in Plasmodium falciparum malaria. *N Engl J Med* **361**, 455-467 (2009).
8. Kuhen, K.L.*, et al.* KAF156 is an antimalarial clinical candidate with potential for use in prophylaxis, treatment, and prevention of disease transmission. *Antimicrobial agents and chemotherapy* **58**, 5060-5067 (2014).
9. Meister, S.*, et al.* Imaging of Plasmodium liver stages to drive next-generation antimalarial drug discovery. *Science* **334**, 1372-1377 (2011).
10. Plouffe, D.*, et al.* In silico activity profiling reveals the mechanism of action of antimalarials discovered in a high-throughput screen. *Proc Natl Acad Sci U S A* **105**, 9059-9064 (2008).
11. Nagle, A.*, et al.* Imidazolopiperazines: lead optimization of the second-generation antimalarial agents. *Journal of medicinal chemistry* **55**, 4244-4273 (2012).
12. Wu, T.*, et al.* Imidazolopiperazines: hit to lead optimization of new antimalarial agents. *Journal of medicinal chemistry* **54**, 5116-5130 (2011).
13. Leong, F.J.*, et al.* A first-in-human randomized, double-blind, placebo-controlled, single- and multiple-ascending oral dose study of novel Imidazolopiperazine KAF156 to assess its safety, tolerability, and pharmacokinetics in healthy adult volunteers. *Antimicrob Agents Chemother* **58**, 6437-6443 (2014).

14. White, N.J., *et al.* Antimalarial Activity of KAF156 in Falciparum and Vivax Malaria. *New England Journal of Medicine* **375**, 1152-1160 (2016).
15. Lim, M.Y., *et al.* UDP-galactose and acetyl-CoA transporters as Plasmodium multidrug resistance genes. *Nat Microbiol*, 16166 (2016).
16. Miao, J., *et al.* Extensive lysine acetylation occurs in evolutionarily conserved metabolic pathways and parasite-specific functions during Plasmodium falciparum intraerythrocytic development. *Mol Microbiol* **89**, 660-675 (2013).
17. Ishida, N. & Kawakita, M. Molecular physiology and pathology of the nucleotide sugar transporter family (SLC35). *Pflugers Arch* **447**, 768-775 (2004).
18. Reyes, F., *et al.* AtUTr1, a UDP-glucose/UDP-galactose transporter from Arabidopsis thaliana, is located in the endoplasmic reticulum and up-regulated by the unfolded protein response. *J Biol Chem* **281**, 9145-9151 (2006).
19. Dejima, K., *et al.* The ortholog of human solute carrier family 35 member B1 (UDP-galactose transporter-related protein 1) is involved in maintenance of ER homeostasis and essential for larval development in Caenorhabditis elegans. *Faseb j* **23**, 2215-2225 (2009).
20. Zhang, M., *et al.* Uncovering the essential genes of the human malaria parasite Plasmodium falciparum by saturation mutagenesis. *Science* **360**(2018).
21. LaMonte, G., *et al.* Mutations in the Plasmodium falciparum Cyclic Amine Resistance Locus (PfCARL) Confer Multidrug Resistance. *MBio* **7**(2016).
22. Magistrado, P.A., *et al.* Plasmodium falciparum Cyclic Amine Resistance Locus (PfCARL), a Resistance Mechanism for Two Distinct Compound Classes. *ACS Infectious Diseases* (2016).
23. Zhang, S., Xu, C., Larrimore, K.E. & Ng, D.T.W. Slp1-Emp65: A Guardian Factor that Protects Folding Polypeptides from Promiscuous Degradation. *Cell* **171**, 346-357.e312 (2017).
24. Allman, E.L., Painter, H.J., Samra, J., Carrasquilla, M. & Llinas, M. Metabolomic Profiling of the Malaria Box Reveals Antimalarial Target Pathways. *Antimicrob Agents Chemother* (2016).
25. Suzuki, Y., *et al.* Knocking out multigene redundancies via cycles of sexual assortment and fluorescence selection. *Nat Methods* **8**, 159-164 (2011).
26. Goldgof, G.M., *et al.* Comparative chemical genomics reveal that the spiroindolone antimalarial KAE609 (Cipargamin) is a P-type ATPase inhibitor. *Scientific reports* **6**, 27806 (2016).
27. LaMonte, G.M., *et al.* Development of a Potent Inhibitor of the Plasmodium Proteasome with Reduced Mammalian Toxicity. *Journal of medicinal chemistry* **60**, 6721-6732 (2017).
28. Feldheim, D., Yoshimura, K., Admon, A. & Schekman, R. Structural and functional characterization of Sec66p, a new subunit of the polypeptide translocation apparatus in the yeast endoplasmic reticulum. *Mol Biol Cell* **4**, 931-939 (1993).
29. David, D., Sundararabu, S. & Gerst, J.E. Involvement of long chain fatty acid elongation in the trafficking of secretory vesicles in yeast. *J Cell Biol* **143**, 1167-1182 (1998).
30. Protopopov, V., Govindan, B., Novick, P. & Gerst, J.E. Homologs of the synaptobrevin/VAMP family of synaptic vesicle proteins function on the late secretory pathway in S. cerevisiae. *Cell* **74**, 855-861 (1993).
31. Winzeler, E.A., *et al.* Functional characterization of the S. cerevisiae genome by gene deletion and parallel analysis. *Science* **285**, 901-906 (1999).
32. Giaever, G., *et al.* Functional profiling of the Saccharomyces cerevisiae genome. *Nature* **418**, 387-391 (2002).
33. Friederichs, J.M., *et al.* Genetic analysis of Mps3 SUN domain mutants in Saccharomyces cerevisiae reveals an interaction with the SUN-like protein Slp1. *G3 (Bethesda)* **2**, 1703-1718 (2012).
34. Heung, L.J., Luberto, C. & Del Poeta, M. Role of sphingolipids in microbial pathogenesis. *Infect Immun* **74**, 28-39 (2006).
35. McQueen, A., *et al.* Synthesis, characterization, and cellular localization of a fluorescent probe of the antimalarial 8-aminoquinoline primaquine. *Bioorganic & medicinal chemistry letters* **27**, 4597-4600 (2017).

36. Alexander, M.D., *et al.* A central strategy for converting natural products into fluorescent probes. *Chembiochem : a European journal of chemical biology* **7**, 409-416 (2006).
37. Labaied, M., *et al.* Anti-Plasmodium activity of ceramide analogs. *Malaria journal* **3**, 49 (2004).
38. Helms, J.B. & Rothman, J.E. Inhibition by brefeldin A of a Golgi membrane enzyme that catalyses exchange of guanine nucleotide bound to ARF. *Nature* **360**, 352 (1992).
39. Saenz, J.B., *et al.* Golgicide A reveals essential roles for GBF1 in Golgi assembly and function. *Nature chemical biology* **5**, 157-165 (2009).
40. Oslowski, C.M. & Urano, F. Measuring ER stress and the unfolded protein response using mammalian tissue culture system. *Methods in enzymology* **490**, 71-92 (2011).
41. Boddey, J.A., *et al.* An aspartyl protease directs malaria effector proteins to the host cell. *Nature* **463**, 627-631 (2010).
42. Hodder, A.N., *et al.* Structural basis for plasmepsin V inhibition that blocks export of malaria proteins to human erythrocytes. *Nature Structural &Amp; Molecular Biology* **22**, 590 (2015).
43. Collins, C.R., Hackett, F., Atid, J., Tan, M.S.Y. & Blackman, M.J. The Plasmodium falciparum pseudoprotease SERA5 regulates the kinetics and efficiency of malaria parasite egress from host erythrocytes. *PLOS Pathogens* **13**, e1006453 (2017).
44. Prommana, P., *et al.* Inducible knockdown of Plasmodium gene expression using the glmS ribozyme. *PLoS One* **8**, e73783 (2013).
45. Marapana, D.S., *et al.* Plasmepsin V cleaves malaria effector proteins in a distinct endoplasmic reticulum translocation interactome for export to the erythrocyte. *Nat Microbiol* **3**, 1010-1022 (2018).
46. Waller, R.F., Reed, M.B., Cowman, A.F. & McFadden, G.I. Protein trafficking to the plastid of Plasmodium falciparum is via the secretory pathway. *The EMBO Journal* **19**, 1794-1802 (2000).
47. Adjalley, S.H., Lee, M.C. & Fidock, D.A. A method for rapid genetic integration into Plasmodium falciparum utilizing mycobacteriophage Bxb1 integrase. *Methods Mol Biol* **634**, 87-100 (2010).
48. Elmendorf, H.G. & Haldar, K. Identification and localization of ERD2 in the malaria parasite Plasmodium falciparum: separation from sites of sphingomyelin synthesis and implications for organization of the Golgi. *Embo j* **12**, 4763-4773 (1993).
49. Staines, H.M., *et al.* Solute transport via the new permeability pathways in Plasmodium falciparum–infected human red blood cells is not consistent with a simple single-channel model. *Blood* **108**, 3187-3194 (2006).
50. Bunnik, E.M., *et al.* Polysome profiling reveals translational control of gene expression in the human malaria parasite Plasmodium falciparum. *Genome biology* **14**, R128 (2013).
51. Boddey, J.A., *et al.* Role of plasmepsin V in export of diverse protein families from the Plasmodium falciparum exportome. *Traffic (Copenhagen, Denmark)* **14**, 532-550 (2013).
52. McNamara, C.W., *et al.* Targeting Plasmodium PI(4)K to eliminate malaria. *Nature* **504**, 248-253 (2013).
53. Fujita, E., *et al.* Two endoplasmic reticulum-associated degradation (ERAD) systems for the novel variant of the mutant dysferlin: ubiquitin/proteasome ERAD(I) and autophagy/lysosome ERAD(II). *Hum Mol Genet* **16**, 618-629 (2007).
54. Peng, Y., *et al.* Deficient import of acetyl-CoA into the ER lumen causes neurodegeneration and propensity to infections, inflammation, and cancer. *J Neurosci* **34**, 6772-6789 (2014).
55. Bernales, S., McDonald, K.L. & Walter, P. Autophagy counterbalances endoplasmic reticulum expansion during the unfolded protein response. *PLoS Biol* **4**, e423 (2006).
56. McLaughlin, M. & Vandenbroeck, K. The endoplasmic reticulum protein folding factory and its chaperones: new targets for drug discovery? *Br J Pharmacol* **162**, 328-345 (2011).
57. Harbut, M.B., *et al.* Targeting the ERAD pathway via inhibition of signal peptide peptidase for antiparasitic therapeutic design. *Proc Natl Acad Sci U S A* **109**, 21486-21491 (2012).

58. Panchal, M., *et al.* Plasmodium falciparum signal recognition particle components and anti-parasitic effect of ivermectin in blocking nucleo-cytoplasmic shuttling of SRP. *Cell Death & Disease* **5**, e994 (2014).
59. Wu, B.X., Hong, F., Zhang, Y., Ansa-Addo, E. & Li, Z. GRP94/gp96 in Cancer: Biology, Structure, Immunology, and Drug Development. *Advances in cancer research* **129**, 165-190 (2016).
60. Mayer, M., Reinstein, J. & Buchner, J. Modulation of the ATPase cycle of BiP by peptides and proteins. *Journal of molecular biology* **330**, 137-144 (2003).
61. Gestwicki, J.E. & Shao, H. Inhibitors and chemical probes for molecular chaperone networks. *J Biol Chem* **294**, 2151-2161 (2019).
62. Colanzi, A., *et al.* Molecular mechanism and functional role of brefeldin A-mediated ADP-ribosylation of CtBP1/BARS. *Proc Natl Acad Sci U S A* **110**, 9794-9799 (2013).
63. Magistrado, P.A., *et al.* Plasmodium falciparum Cyclic Amine Resistance Locus (PfCARL), a Resistance Mechanism for Two Distinct Compound Classes. *ACS Infect Dis* **2**, 816-826 (2016).
64. Antonova-Koch, Y., *et al.* Open-source discovery of chemical leads for next-generation chemoprotective antimalarials. *Science* **362**, eaat9446 (2018).
65. Fumagalli, F., *et al.* Translocon component Sec62 acts in endoplasmic reticulum turnover during stress recovery. *Nat Cell Biol* **18**, 1173-1184 (2016).
66. Paquet, T., *et al.* Antimalarial efficacy of MMV390048, an inhibitor of Plasmodium phosphatidylinositol 4-kinase. *Sci Transl Med* **9**(2017).
67. Martinez Molina, D., *et al.* Monitoring drug target engagement in cells and tissues using the cellular thermal shift assay. *Science* **341**, 84-87 (2013).
68. Hoepfner, D., *et al.* Selective and specific inhibition of the plasmodium falciparum lysyl-tRNA synthetase by the fungal secondary metabolite cladosporin. *Cell Host Microbe* **11**, 654-663 (2012).
69. Li, H. & Durbin, R. Fast and accurate short read alignment with Burrows-Wheeler transform. *Bioinformatics* **25**, 1754-1760 (2009).
70. McKenna, A., *et al.* The Genome Analysis Toolkit: a MapReduce framework for analyzing next-generation DNA sequencing data. *Genome Res* **20**, 1297-1303 (2010).
71. Cingolani, P., *et al.* A program for annotating and predicting the effects of single nucleotide polymorphisms, SnpEff: SNPs in the genome of Drosophila melanogaster strain w1118; iso-2; iso-3. *Fly* **6**, 80-92 (2012).
72. Ottilie, S., *et al.* Rapid Chagas Disease Drug Target Discovery Using Directed Evolution in Drug-Sensitive Yeast. *ACS Chem Biol* **12**, 422-434 (2017).
73. Trager, W. & Jensen, J.B. Human malaria parasites in continuous culture. *Science* **193**, 673-675 (1979).
74. Johnson, J.D., *et al.* Assessment and continued validation of the malaria SYBR green I-based fluorescence assay for use in malaria drug screening. *Antimicrob Agents Chemother* **51**, 1926-1933 (2007).
75. Maier, A.G., *et al.* Exported proteins required for virulence and rigidity of Plasmodium falciparum-infected human erythrocytes. *Cell* **134**, 48-61 (2008).
76. Rottmann, M., *et al.* Spiroindolones, a potent compound class for the treatment of malaria. *Science* **329**, 1175-1180 (2010).
77. Nkrumah, L.J., *et al.* Efficient site-specific integration in Plasmodium falciparum chromosomes mediated by mycobacteriophage Bxb1 integrase. *Nat Methods* **3**, 615-621 (2006).
78. Suzuki, Y., *et al.* The green monster process for the generation of yeast strains carrying multiple gene deletions. *J Vis Exp*, e4072 (2012).
79. Walliker, D., *et al.* Genetic analysis of the human malaria parasite Plasmodium falciparum. *Science* **236**, 1661-1666 (1987).
80. Guinet, F., *et al.* A developmental defect in Plasmodium falciparum male gametogenesis. *J Cell Biol* **135**, 269-278 (1996).

933 81. Liu, W., *et al.* IBS: an illustrator for the presentation and visualization of biological sequences.
934 *Bioinformatics* **31**, 3359-3361 (2015).
935 82. Szklarczyk, D., *et al.* STRING v10: protein-protein interaction networks, integrated over the tree
936 of life. *Nucleic Acids Res* **43**, D447-452 (2015).
937

938

TABLES

Standard and Systematic Gene Name	Strain/Clone Name	Amino Acid Change	GNF179 IC_{50} (uM)	GNF179 Fold resistance (FR)
N/A	ABC_{16}-Monster-Parent	N/A	45.39 ± 5.7	N/A
ELO2 (YCR034W) Fatty acid elongase, involved in sphingolipid biosynthesis	GNF179-R9-2	G183C	81.18 + 6.3	1.8
	GNF179-R10-2	G183C	90.31 ± 14.8	2.0
	GNF179-R18g1	L193W	137.66 ± 5.1	3.0
	GNF179-R8h2	L169R	138.05*	3.0
	GNF179-R9f2	A186D	94.7 ± 41.3	2.1
SUR2 (YDR297W) Sphinganine C4-hydroxylase	GNF179-R18g1	S94*	137.66 ± 5.1	3.0
	GNF179-R19g2	D257Y	109.35 ± 23.1	2.4
	GNF179-R9f2	I108K	94.7 ± 41.3	2.1
ATG15(YCR068W) Phospholipase	GNF179-R18g1	W200*	137.66 ± 5.1	3.0
	GNF179-R19g2	C271Y	109.35 ± 23.1	2.4
	GNF179-R9f2	W380*	94.7 ± 41.3	2.1
	GNF179-R8h2	K303fs	138.05*	3.0
LCB4 (YOR171C) Shingoid long-chain base kinase	GNF179-R9f2	Y421N/A423S	94.7 ± 41.3	2.1
	GNF179-R8h2	T336K	138.05*	3.0
YMR102C Protein of unknown function	GNF179-R19g2	S448W	109.35 ± 23.1	2.4
	GNF179-R9f2	F381V	94.7 ± 41.3	2.1
	GNF179-R18g1	L271fs	137.66 ± 5.1	3.0
	GNF179-R8h2	Q98fs	138.05*	3.0
SEC66 (YBR171W) Non-essential subunit of Sec63 complex	GNF179-R1-2	S107*	80.12 ± 14.6	1.8
	GNF179-R12-2	M1I	67.22 ± 10.4	1.5

Table 1. Mutations identified in more than one GNF179-resistant *S. cerevisiae* line, from a pool of 13 evolved strains. 18 hrs IC_{50s} against GNF179 (mean ± standard error with $n \geq 2$) and fold resistances (calculated relative to the parental ABC_{16}-Monster-Parent strain) are indicated. The complete set of coding changes for the 13 resistant lines are given in Table S1. *Replicate not available.

948
949
950

Strain Name	Systematic Gene ID	Standard Gene Name	Mutation	Gene Description	GNF179 IC_{50} (μM)	GNF179 Fold resistance (FR)
ABC_{16}-Monster	N/A	N/A	N/A	N/A	47.30 ± 3.8	N/A
EAW361	YBR171W	*SEC66*	M1I	Non-essential subunit of Sec63 complex, involved in protein targeting and import into the ER	70.10 ± 11.7	1.5
EAW277	YBR171W	*SEC66*	S107*	Non-essential subunit of Sec63 complex, involved in protein targeting and import into the ER	74.83 ± 9.4	1.6
EAW289	YCR034W	*ELO2*	G183C	Fatty acid elongase, involved in sphingolipid biosynthesis;	88.15 ± 8.7	1.9
EAW327	YLR372W	*ELO3*	Y307*	Fatty acid elongase, involved in sphingolipid biosynthesis;	76.57 ± 10.0	1.6

951 **Table 2. IC_{50s} (mean and S.E.M) for GNF179 in the indicated yeast CRISPR-*Cas9* edited strains.** Strain name,
952 systematic name, 18h IC_{50s} against GNF179 (mean ± standard error with $n \geq 3$) and relative change compared to
953 unedited ABC_{16}-Monster strain are indicated.
954

Strain Name	Systematic Name	Mutation	Gene Description	GNF179 IC_{50} (nM)	GNF179-fold resistance (FR)
BY4742	N/A	N/A	N/A	121.26 ± 2.9	N/A
sec66Δ	YBR171W	*Haploid deletion of sec66*	Non-essential subunit of Sec63 complex, involved in protein targeting and import into the ER	188.69 ± 11.4	1.6
sec72Δ	YLR292C	*Haploid deletion of sec72*	Non-essential subunit of Sec63 complex, involved in protein targeting and import into the ER	177.37 ± 5.1	1.5
elo2Δ	YCR034W	Haploid deletion of *elo2*	Fatty acid elongase, involved in sphingolipid biosynthesis;	254.88 ± 55.1	2.1
sur2Δ	YDR297W	Haploid deletion of *sur2*	Sphinganine C4-hydroxylase; catalyses the conversion of sphinganine to phytosphingosine	217.9 ± 12.5	1.8
emp65Δ	YER140W	Haploid deletion of *emp65*	Integral membrane protein of the ER	152.2 ± 10.5	1.3
atg15Δ	YCR068W	Haploid deletion of *atg15*	Phospholipase	137.54 ± 12.9	1.1

Table 3. IC_{50}s (mean and S.E.M) for GNF179 in the indicated yeast haploid deletion strains. Strain name, systematic name, 18h IC_{50} against GNF179 (mean ± standard error with $n \geq 2$) and relative change compared to wild-type are indicated. Strains obtained from yeast deletion collection.[31]

Plasmodium falciparum Drug Treatment	GNF179 IC_{50} (nM)	Fold Change in IC_{50}	Artemisinin IC_{50} (nM)	Chloroquine IC_{50} (nM)
Dd2	4.31 ± 0.88	-	19.4 ± 1.2	117 ± 14
Dd2 + 1 μM Brefeldin A	0.80 ± 0.22	0.19	21.1 ± 2.7	108.1 ± 17
Dd2 + 5 uM Golgicidin	1.55 ± 0.3	0.36	20.4 ± 1.9	108 ± 18
Dd2 + 250 nM KDU691	1.8 ± 0.35	0.42	18.0 ± 2.4	90.3 ± 6
Dd2 + 1 mM Thapsigargin	4.42 ± 1.4	1.3	18.4 ± 0.8	139 ± 9.8
Dd2 + 1 nM Carmaphycin B	2.6 ± 0.1	0.75	3.5 ± 1.2	90 ± 5.8
Dd2 + 100 nM Cycloheximide	2.6 ± 0.63	0.75	17.5 ± 1.52	101 ± 13.1

Table 4. 72-hour SYBR-green IC_{50}s for the indicated compound combinations including GNF179. Parasites were synchronized to ring stage before IC_{50}s were measured using the SYBR green method. IC_{50}s presented as Mean ± Standard Error with ≥2 biological replicates of two technical replicates each.

Strain	**Species**	**Genotype**	**Method or Ref.**
ABC_{16}-Monster	Sc	*MATa adp1Δ snq2Δ ycf1Δ pdr15Δ yor1Δ vmr1Δ pdr11Δ nft1Δ bpt1Δ ybt1Δ ynr070wΔ yol075cΔ aus1Δ pdr5Δ pdr10Δ pdr12can1Δ::*GMToolkit-**a** *lyp1Δ his3Δ1 leu2Δ0 ura3Δ0 met15Δ0* (deletions for the ABC transporter genes are marked with *[tetO$_2$pr-GFP, URA3]*).	[78]
BY4742		*MATα his3Δ1 leu2Δ0 lys2Δ0 ura3Δ0*	
Sec66Δ	Sc	*MATα his3Δ1 leu2Δ0 lys2Δ0 ura3Δ0 sec66::KANMX4*	[31,32]
Sec72Δ	Sc	*MATα his3Δ1 leu2Δ0 lys2Δ0 ura3Δ0 sec72::KANMX4*	[31,32]
Elo2Δ	Sc	*MATα his3Δ1 leu2Δ0 lys2Δ0 ura3Δ0 elo2::KANMX4*	[31,32]
Sur2Δ	Sc	*MATα his3Δ1 leu2Δ0 lys2Δ0 ura3Δ0 sur2::KANMX4*	[31,32]
Atg15Δ	Sc	*MATα his3Δ1 leu2Δ0 lys2Δ0 ura3Δ0 atg15::KANMX4*	[31,32]
GNF179-G72	Sc	ABC_{16}-Monster	Evolved
GNF179-R1-2	Sc	ABC_{16}-Monster	Evolved
GNF179-R10-2	Sc	ABC_{16}-Monster	Evolved
GNF179-R12-2	Sc	ABC_{16}-Monster	Evolved
GNF179-R12h2	Sc	ABC_{16}-Monster	Evolved
GNF179-R13-2	Sc	ABC_{16}-Monster	Evolved
GNF179-R14-2	Sc	ABC_{16}-Monster	Evolved
GNF179-R18g1	Sc	ABC_{16}-Monster	Evolved
GNF179-R19g2	Sc	ABC_{16}-Monster	Evolved
GNF179-R7-2	Sc	ABC_{16}-Monster	Evolved
GNF179-R8h2	Sc	ABC_{16}-Monster	Evolved
GNF179-R9-2	Sc	ABC_{16}-Monster	Evolved
GNF179-R9f2	Sc	ABC_{16}-Monster	Evolved
EAW289	Sc	ABC_{16}-Monster	Edited
EAW327	Sc	ABC_{16}-Monster	Edited
EAW361	Sc	ABC_{16}-Monster	Edited
EAW277	Sc	ABC_{16}-Monster	Edited
3D7	Pf		[79]
Dd2	Pf	*Pfcrt* (K76T), *pfmdr1* (CNV)	[80]
KAD452-R3	Pf	Dd2 *pfcarl* (M81I, L830V and S1076I)	Evolved
Dd2-ACTStop	Pf	Dd2 *pfact (S242*)*	Edited [21]
Dd2attB KAHRP69-GFP	Pf	Dd2 *attB::KAHRP69-GFP*	Recom-binannt

988 **Table 5. Strains used in this study**. Sc, *S. cerevisiae*, Pf, *P. falciparum*.

989

FIGURES

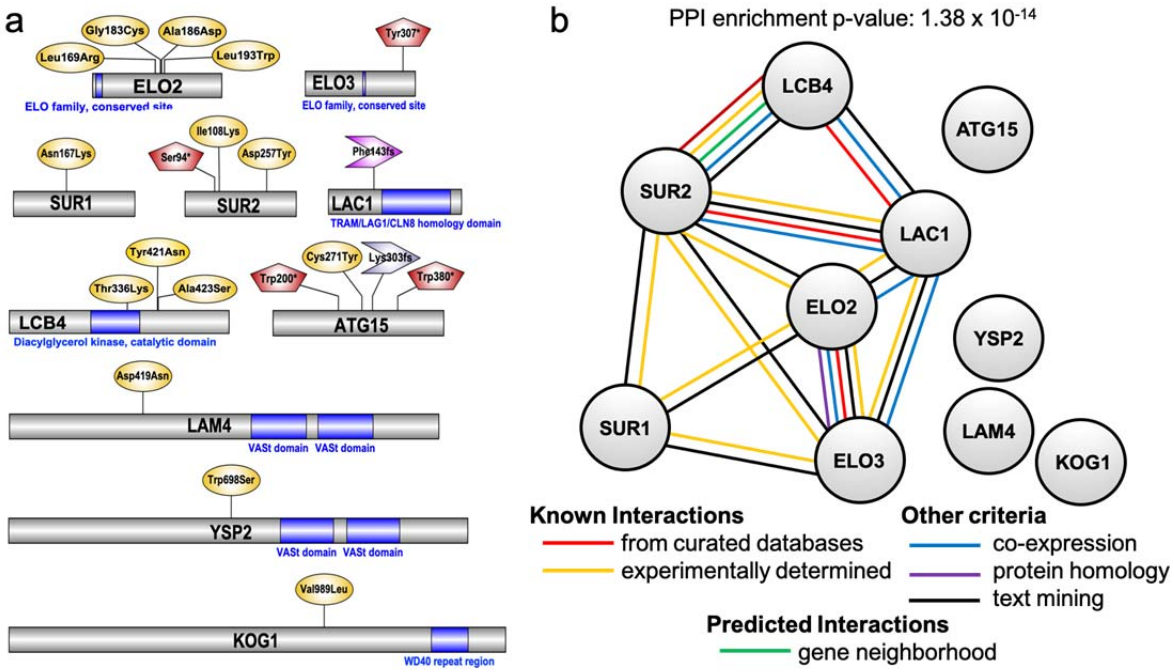

Figure 1. GNF179-resistant yeast strains harbor mutations in endoplasmic reticulum(ER)-based lipid homeostasis and autophagy. (a) Protein maps showing relevant mutations and PROSITE predicted protein domains, if applicable. Maps were generated using Illustrator of Biological Sequences (IBS) software package.[81] Missense mutations are shown in yellow ovals, nonsense mutations in red pentagons, and frameshift mutations as purple arrow. (b) Protein-Protein Interaction (PPI) network generated using the STRING database.[82] Each node represents a *S. cerevisiae* protein and connecting lines delineate interactions. The PPI enrichment p-value ($p = 1.38 \times 10^{-14}$) indicates that the proteins show significantly more interactions among themselves than would be expected from a random subset of genes from the yeast genome.

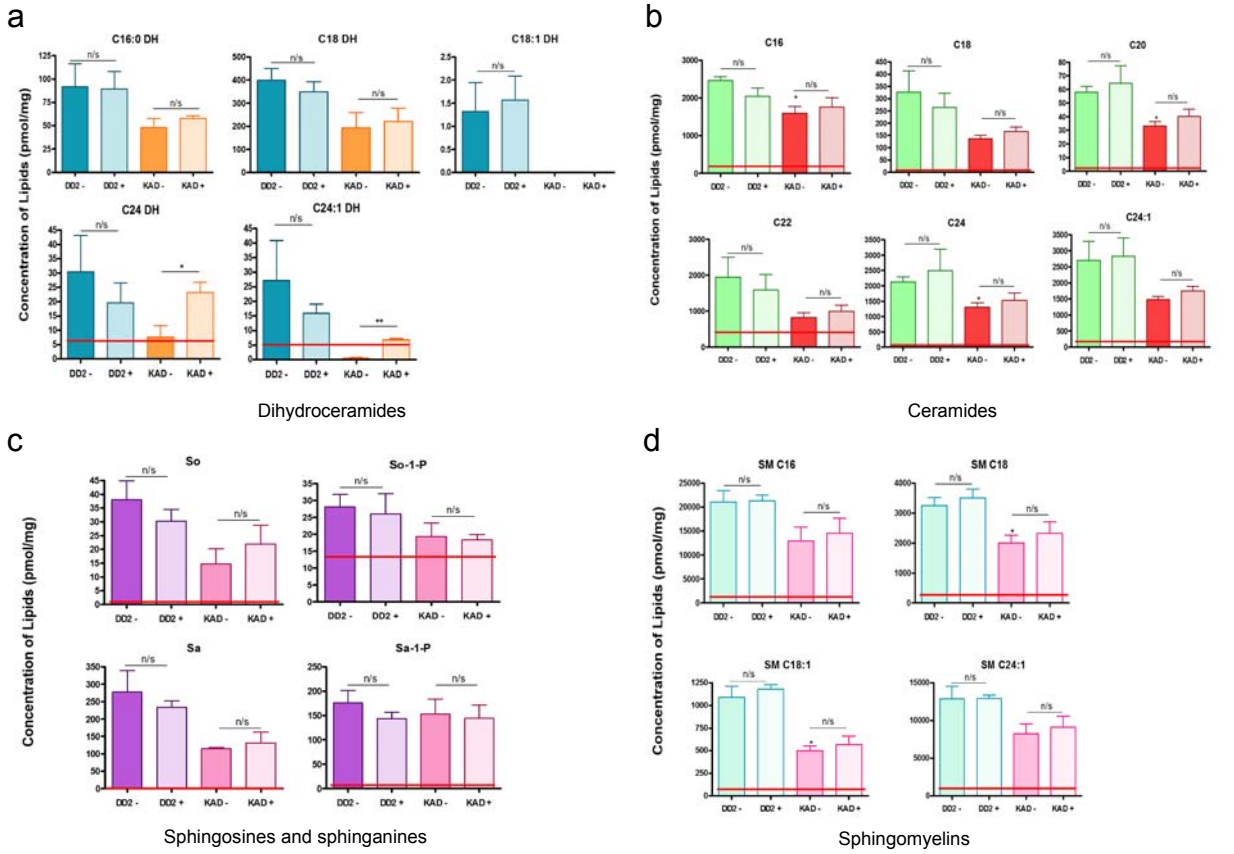

Figure 2. Sphingolipid profile of isolated *P. falciparum*: Wild Type and PfCARL Mutant. Composite profile of 19 sphingolipids from untreated wild type dd2 (DD2-) and *pfcarl* triple mutant (KAD452-R3: M81I, L830V and S1076I) as well as parasites treated with 25nM GNF179 (DD2+, KAD+). Lipids were normalized to protein and reported with SEM indicated by the error bars (n=3 independent experiments). Student's t-test was employed with significance between untreated and treated wild-type and mutant indicated by solid black lines. Significance of all populations with respect to the untreated wild type is indicated by * where $p < 0.05$. Sphingolipid profile comprises (A) dihydroceramides (DH), (B) ceramides (C), (C) sphingosine (So), sphingosine-1-phosphate (So-1-P), sphinganine (Sa), sphinganine1-phosphate (Sa-1-P) and (D) sphingomyelins (SM) with varying fatty acid chains and degrees of saturation. Solid red line represents uninfected red blood cells as a control.

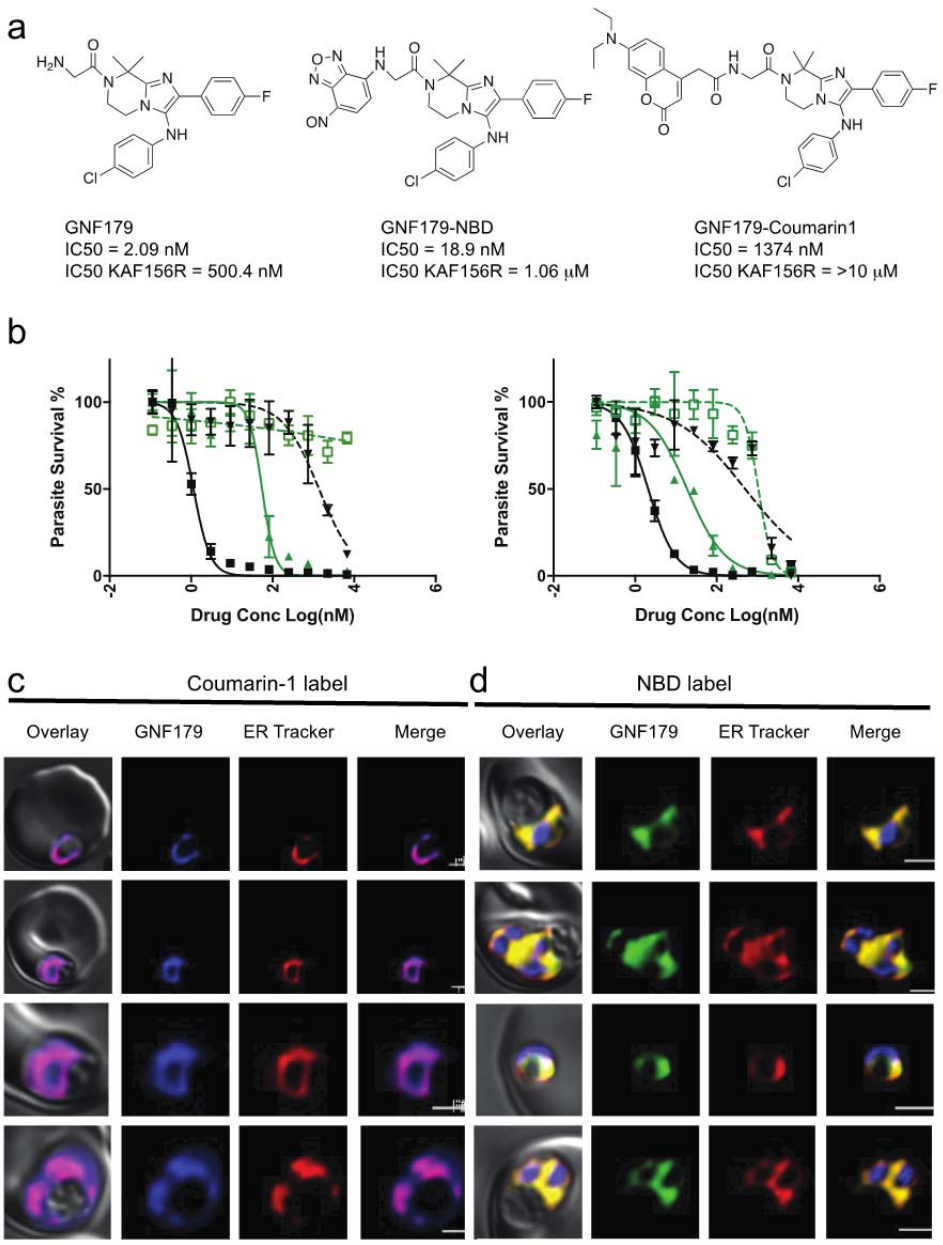

Figure 3. GNF179 localizes to the ER of early stage parasites and interacts with several proteins required for parasite protein trafficking into the ER. (a) Chemical structure of canonical and NBD conjugated GNF179 and Coumarin-1 conjugated GNF179. (b) Dose response curves for GNF179 and Coumarin1 (left) or NBD (right) conjugated GNF179 in wild-type and KAF156-resistant clone (KAD452-R3, containing three mutations in *pfcarl* (M81I, L830V and S1076I). (c) Colocalization of Coumarin-1 conjugated GNF179 with ER-tracker red (d) Colocalization of NBD conjugated GNF179 with ER-tracker red. Parasites are in mid-ring (6-hours post-infection) stage and were treated for 30 minutes with 2 μM GNF179-Coumarin1 and 100 nM GNF179-NBD.

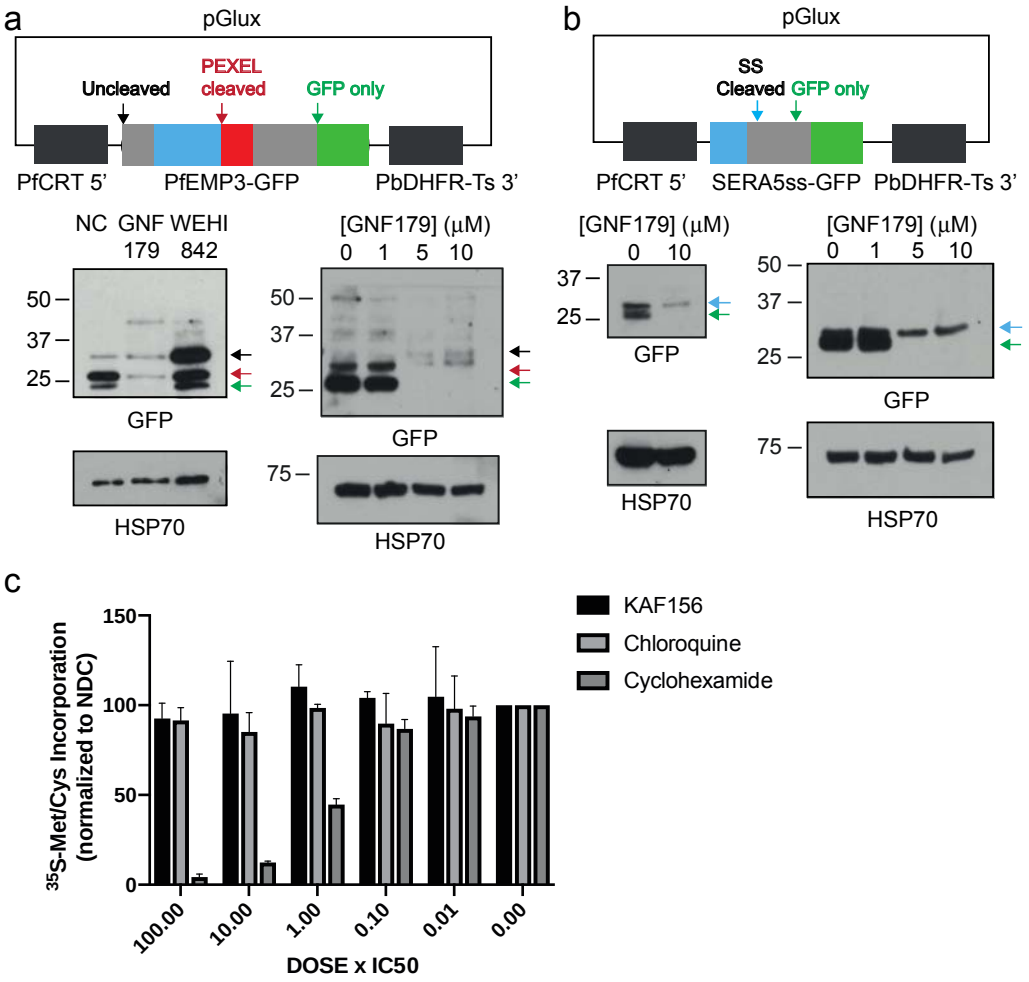

1034

1035 **Figure 4. Secretion reporter constructs demonstrate that GNF179 inhibits protein export**
1036 **of *Plasmodium* falciparum.** (a) Protein expression levels of PfEMP3-GFP reporter. This fusion
1037 includes the signal peptide and PEXEL motif of PfEMP3. By immunoblot, 3 protein products are
1038 seen with anti-GFP antibodies. The three indicated bands, in response to probing with GFP, as
1039 follows: 1. Full length protein (Black arrow), 2. PEXEL cleaved protein (red arrow), 3. GFP
1040 degradation product (green arrow). HSP70 is used as a loading control. (b) SERA5ss-GFP fusion
1041 reporter treated with GNF179. By immunoblot with anti-GFP antibodies we see two protein
1042 products for this construct: 1. Signal peptide cleaved (blue arrow) and 2. GFP degradation
1043 product (green arrow). HSP70 serves as a loading control. (c) ^{35}S incorporation of newly
1044 synthesized amino acids at different concentrations of KAF156, chloroquine (negative control
1045 for inhibition) and cycloheximide (positive control for inhibition). Counts were normalized to
1046 data obtained from no-drug controls (NDC).

1047

1048

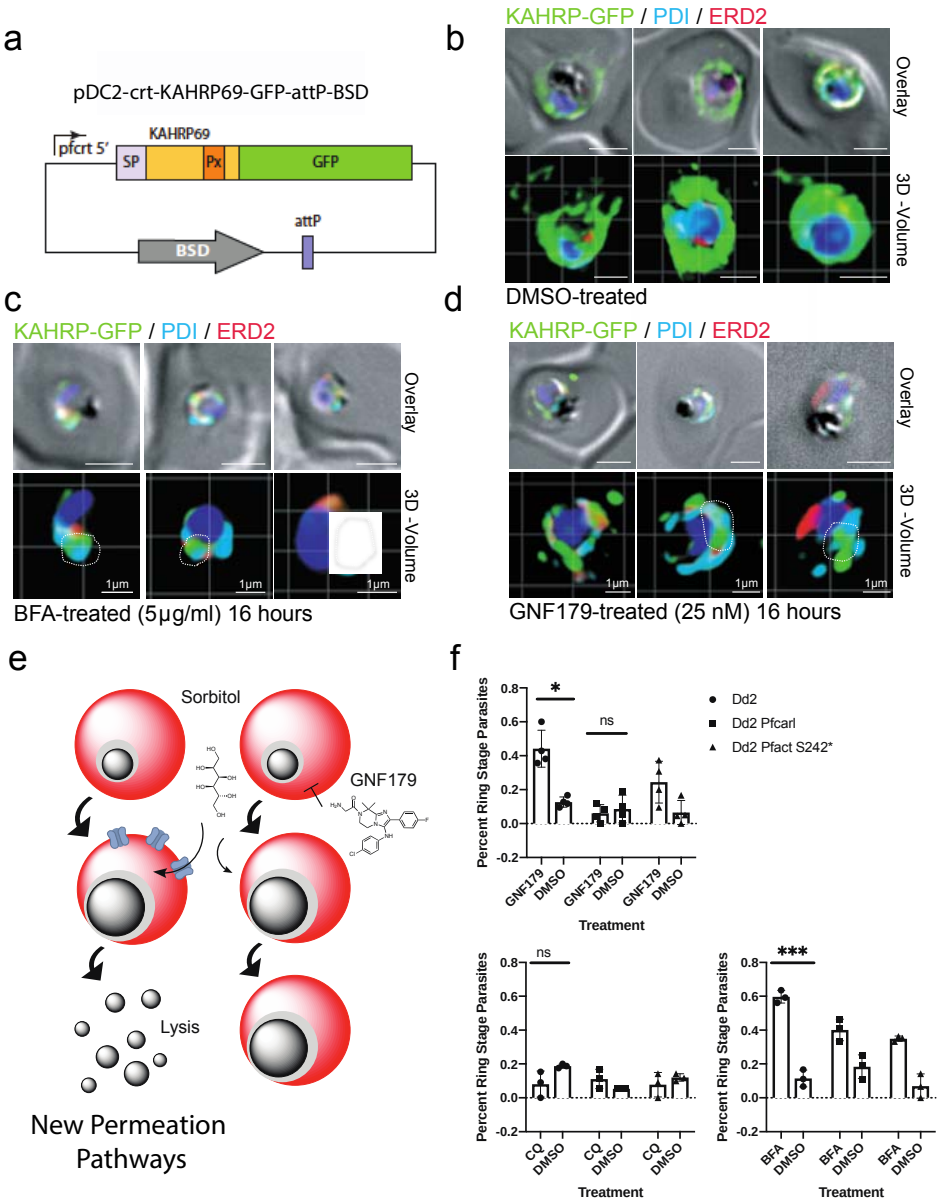

1049

1050 **Figure 5. Confirmation of GNF179's inhibition of protein export in *P. falciparum* blood**
1051 **stage parasites**. (a) Vector used for assays shown in b, c., d. (b, d) Imaging of GFP reporter to
1052 the plasma membrane under the indicated compound treatments for 16 hours. Parasites were
1053 fixed and stained with Hoechst 33342 (blue), α-GFP (green), α-ERD2 (red) and α-PDI (cyan)
1054 antibodies. Scale bars: 2 µm unless otherwise indicated. Overlay: DIC images merged with
1055 fluorescent channels. (e) Model for establishing new permeation pathways. If proteins are not
1056 exported to the red cell where they can form new permeation pathways, sorbitol will not be
1057 imported and cause lysis. (f). Percentage of trophozoites from an asynchronous parasite
1058 population 24 hours after sorbitol synchronization, treated as indicated by GNF179 (5nM),
1059 Chloroquine (CQ, 500nM) or brefeldin A (BFA, 5µM). Statistical significance was determine
1060 using a paired, two-tailed t-test. Dd2 *pfcarl* experiments were conducted with the *pfcarl* evolved

1061 triple mutant (KAD452-R3)) and edited Dd2-ACTStop mutant. For sensitive parasites (Dd2),
1062 25nM of GNF179 was used, while 1μM was used on resistant parasites.

1063

1064 **SUPPLEMENTAL FIGURES AND TABLES:**

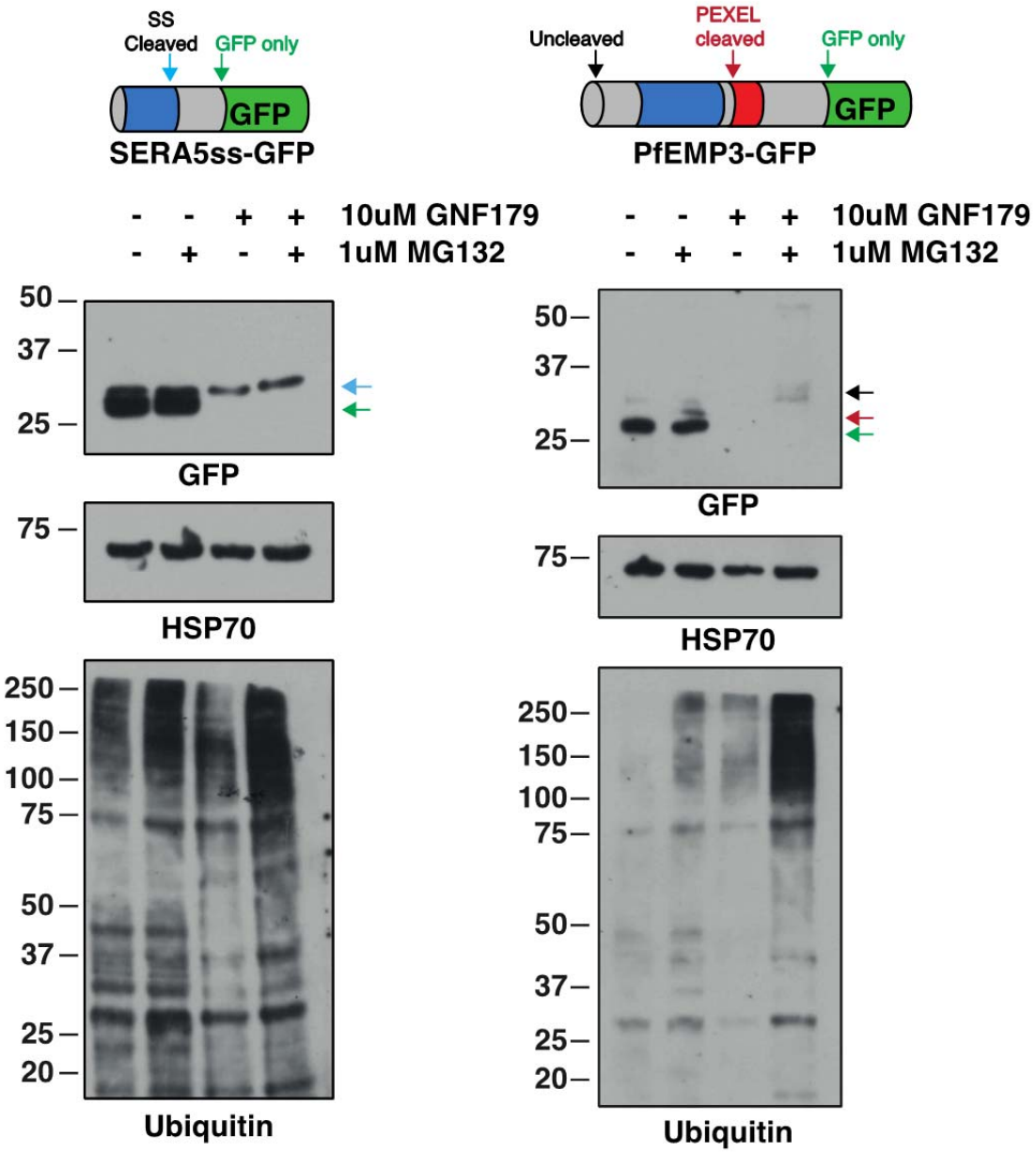

1065

1066 Figure S1. does not induce a significant ubiquitin response in *P. falciparum*. Western blots of *P.*
1067 *falciparum* strains expressing SERA5ss-GFP or PfEMP3-GFP treated with 10uM GNF179
1068 and/or 10µM MG132 for 3 hours were probed with anti-GFP, anti-HSP70 and anti-Ubiquitin
1069 antibodies. For the secreted SERA5ss-GFP reporter, the blue arrow indicates the signal-sequence
1070 cleaved form and the green arrow indicates the GFP-only species. For the exported PfEMP3-
1071 GFP reporter, the black, red and green arrows indicate the full-length, PEXEL-cleaved and GFP
1072 only species respectively.

1073

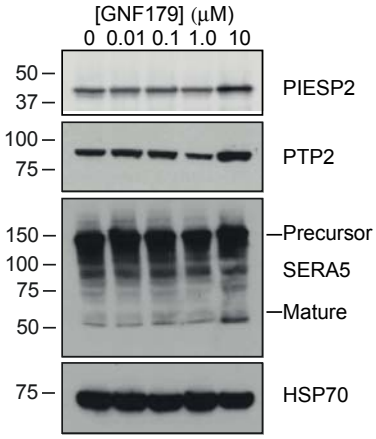

Figure S2. Western blot showing effects by a 3-hour pulse of increasing concentrations of GNF179 on known ER-trafficked proteins in P. falciparum. PIESP2 and PTP2 are examples of PEXEL-containing exported proteins. SERA5 is a secreted protein while HSP70 is a cytosolically expressed protein that lacks a signal sequence required for ER entry.

.

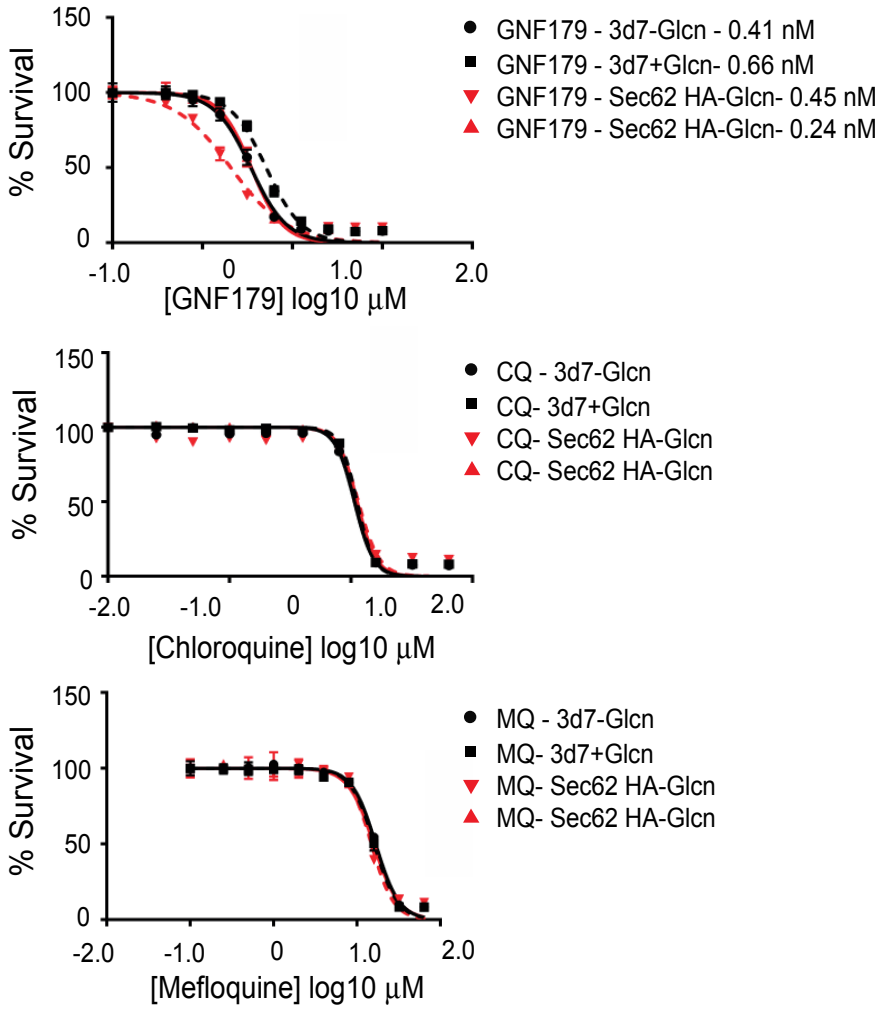

Figure S3. Dose response curves for GNF179 in the SEC62 knockdown parasites, compared to wildtype 3D7 parasites, with and without the addition of N-acetyl Glucosamine (Glcn) for the 3 compounds indicated, GNF179, Chloroquine (CQ) and Mefloquine (MQ). Values are for three independent replicates.

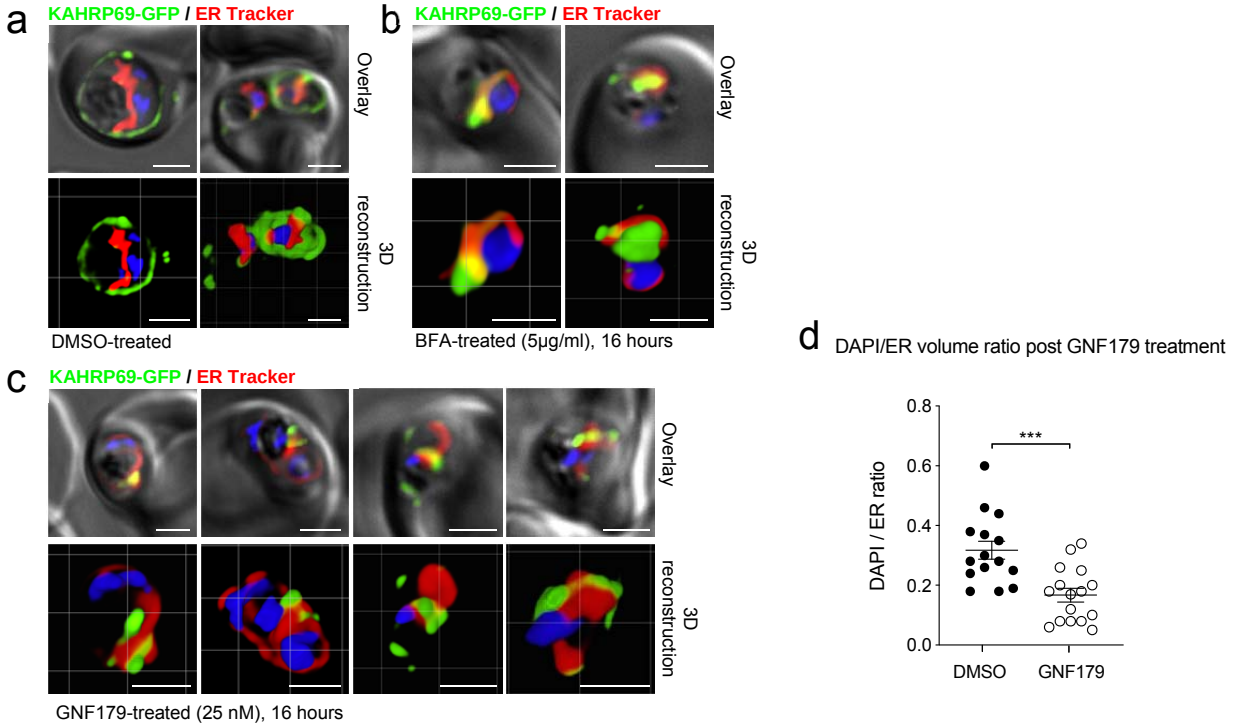

Figure S4. GNF179 treatment increases volume of ER relative to nucleus in Dd2attB KAHRP69-GFP parasites. Red, ER Tracker; Green, GFP; Blue, DAPI. (a) DMSO-treated parasites. (b) Treatment with 5 µg/ml Brefeldin A for 16 hours. (c) Treatment with GNF179 for 16 hours. (d) Quantitation of the 3D Volume ratio of DAPI to ER tracker in 12 images. Statistical significance was determined using a paired, two-tailed t-test. Scale bars: 2 µm

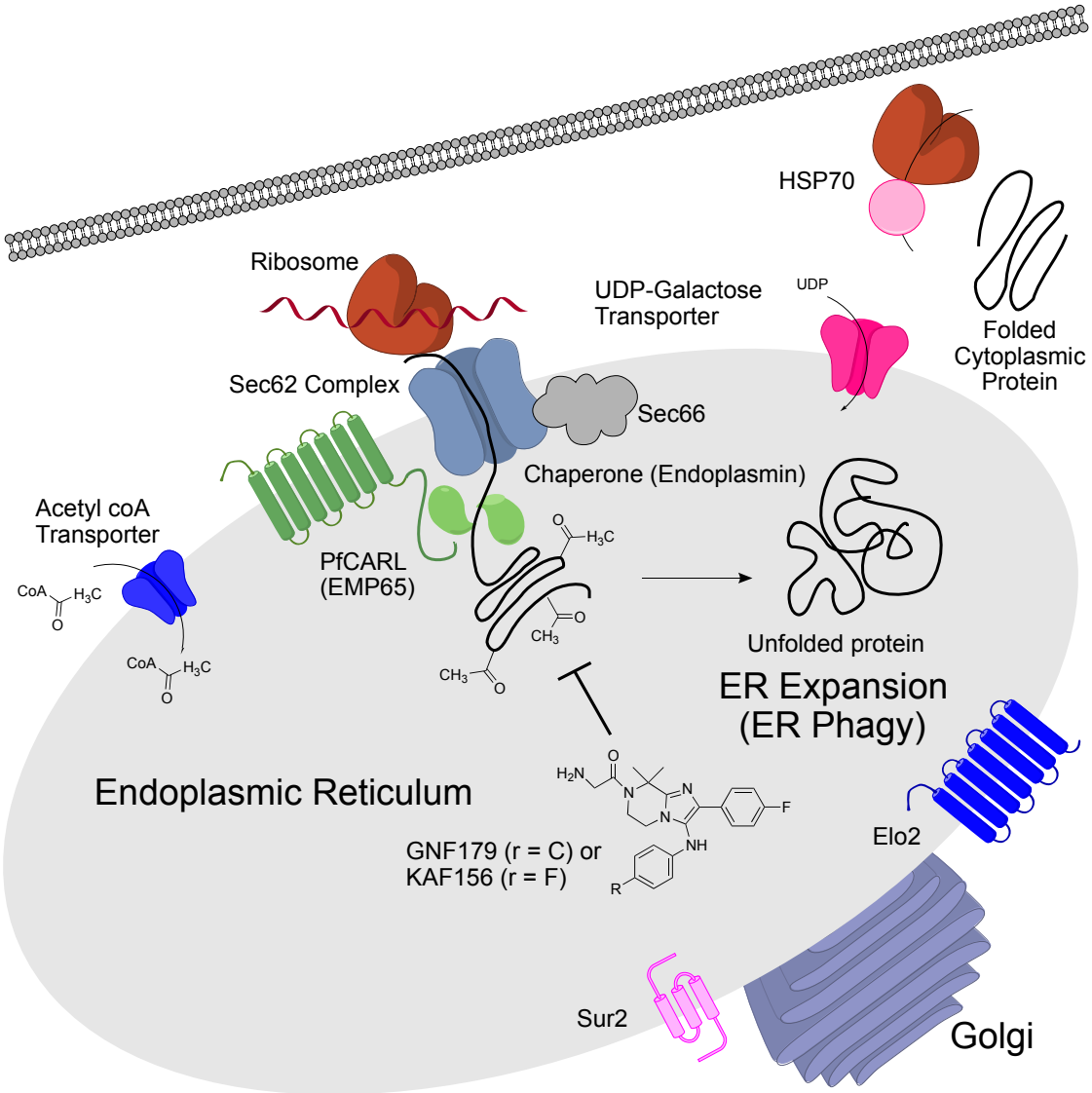

Figure S5. Model that shows how IZP treatment could produce the sets of cellular phenotypes that are observed after treatment. In the model, IZPs inhibit the production of properly folded proteins, potentially by interfering with post-translational modification or folding. Mutations that slow the process of protein processing, as those in the Acetyl Coa transporter, *pfcarl* or *sec66* are beneficial. The accumulation of unprocessed proteins leads to ER expansion. Mutations in the autophagy and sphingolipid pathways (*elo2*, *sur2*) in yeast change the balance of ER phagy, potentially also increasing transit time and providing a slight growth advantage in the presence of GNF179 or KAF156.

Supplemental Tables

Clone Name	Total Base Pairs Sequenced	Mean Coverage (X)	Percent Reads Aligned to Reference	Percent Bases with 20 or More Reads	IC50 (uM)
Green-Monster	557,641,556	42.3	98.7	95.0	45.39 ± 5.7
GNF179-G72	1,085,965,416	59.2	99.2	94.0	63.45 ± 2.6
GNF179-R1-2	483,257,249	31.1	99.1	83.7	80.12 ± 14.6
GNF179-R10-2	868,810,757	49.1	99.4	93.4	90.31 ± 14.8
GNF179-R12-2	1,238,282,174	71.8	99.4	95.0	67.22 ± 10.4
GNF179-R12h2	504,425,192	30.9	99.4	85.3	89.65*
GNF179-R13-2	938,610,879	58.8	99.5	94.4	59.68 ± 11.5
GNF179-R14-2	719,981,126	46.4	99.7	92.0	77.83 ± 7.3
GNF179-R18g1	510,038,211	30.7	99.5	85.2	137.66 ± 5.1
GNF179-R19g2	607,361,091	35.3	99.4	89.1	109.35 ± 23.1
GNF179-R7-2	1,137,607,696	66.7	99.4	94.6	71.11 ± 9.5
GNF179-R8h2	654,463,110	38.2	99.3	90.0	138.05*
GNF179-R9-2	945,657,737	61.3	99.4	94.2	81.18 + 6.3
GNF179-R9f2	697,615,853	40.2	99.4	87.0	94.7 ± 41.3

Table S1. Sequencing and alignment statistics for the 13 GNF179-resistant *S. cerevisiae* strains sequenced in this study. All genome sequences for the 13 IZP-resistant *S. cerevisiae* strains have been placed in the short-read sequence archive (http://www.ncbi.nlm.nih.gov/sra) under accession code STUDY: PRJNA381796 (SRP107357). *Replicate not available

Table S2. Complete set of mutations observed in *S. cerevisiae in vitro* resistance evolutions. (Attached Excel Table) Clone #: The numerical designation for each *S. cerevisiae* GNF179 resistant clone in this study. Chr #: Chromosome # which harbors the identified mutations.

Name	Oligonucleotide Sequence
gRNA Forward Primer Elo2 G183C	tcATAATAAGGCAGTAGCGCCAgTTTTAGAGCTAGAAATAGCAAG
gRNA Reverse Primer Elo2 G183C	aacTGGCGCTACTGCCTTATTATgATCATTTATCTTTCACTGCGGAG
Donor Template Sequence Elo2 G183C	TGCTAAAACATAAAAAATTGACATTTTTGCATACTTATCACCATTGCGCT ACTGCCTTATTATGTTACACCCAATTGATGGGCACCACA
Sequencing Primer Elo2 G183C Coding Strand	GCACGGGTTATACTTCGCTATC
Sequencing Primer Elo2 G183C Non-Coding Strand	CTGGCAGCCAAGAAATAGTACC
gRNA Forward Primer Elo3 Y307*	tcATCCAATCTTACAAGAAAGGgTTTTAGAGCTAGAAATAGCAAG
gRNA Reverse Primer Elo3 Y307*	aacCCTTTCTTGTAAGATTGGATgATCATTTATCTTTCACTGCGGAG
Donor Template Sequence Elo3 Y307*	ACATCTTATTTGCTTTTGTTTATTTCCTTCTACATCCAATCTTAAAAGAAA GGTGGTAAAAAGACAGTCAAGAAGGAATCTGAAGTTTCC
Sequencing Primer Elo3 Y307* Coding Strand	TGTTATGGTACTCAGGCTGCTG
Sequencing Primer Elo3 Y307* Non-Coding Strand	CCTGGAAGAGACCTTGGTGTTA
gRNA Forward Primer Sec66 M1 read through	tcTTCATTAAATTCGGACATATgTTTTAGAGCTAGAAATAGCAAG
gRNA Reverse Primer Sec66 M1 read through	aacATATGTCCGAATTTAATGAAgATCATTTATCTTTCACTGCGGAG
Donor Template Sequence Sec66 M1 read through	AGTACAGGAAAGAGGTACGCACAACTACTTGAGTTTGCCAATATTTCCG AATTTAATGAAACAAAATTCTCCAACAACGGGACGTTTTTT
Sequencing Primer Sec66 M1 read through Coding Strand	GTAGACGCATCTTATTACCCGC
Sequencing Primer Sec66 M1 read through Non-Coding Strand	TGAGTGGGGTATAAACGGAGAT
gRNA Forward Primer Sec66 S107*	tcATCATTAAAGTTAAAAGAGTgTTTTAGAGCTAGAAATAGCAAG
gRNA Reverse Primer Sec66 S107*	aacACTCTTTTAACTTTAATGATgATCATTTATCTTTCACTGCGGAG
Donor Template Sequence Sec66 S107*	GAAGGCCGCTTTATTGAACAGAGGAGCAGAGTCTGTTAGACGATGATTA AAGTTAAAAGAGTTGGCTCCTCAGATAAACCTTCTATATAA
Sequencing Primer Sec66 S107* Coding Strand	CATCCATATTTGACGAAAACGA
Sequencing Primer Sec66 S107* Non-Coding Strand	GGTTGCAATCTTTCAGCTTCTT

Table S3. Oligonucleotides used in this study.